Nuclear Engineering and Design 239 (2009) 2672–2691

Contents lists available at ScienceDirect

Nuclear Engineering and Design

journal homepage: www.elsevier.com/locate/nucengdes

Cross-comparison of fast reactor concepts with various coolants

Pavel Hejzlar[a,*], Neil E. Todreas[a], Eugene Shwageraus[b], Anna Nikiforova[a], Robert Petroski[a], Michael J. Driscoll[a]

[a] Center for Advanced Nuclear Energy Systems, Department of Nuclear Science and Engineering, Massachusetts Institute of Technology, Cambridge, MA 02139, USA
[b] Ben-Gurion University, Beer Sheva 84105, Israel

ARTICLE INFO

ABSTRACT

Four fast reactor concepts using lead (LFR), liquid salt, NaCl–KCl–$MgCl_2$ (LSFR), sodium (SFR), and supercritical CO_2 (GFR) coolants are compared. Since economy of scale and power conversion system compactness are the same by virtue of the consistent 2400 MWt rating and use of the S-CO_2 power conversion system, the achievable plant thermal efficiency, core power density and core specific powers become the dominant factors. The potential to achieve the highest efficiency among the four reactor concepts can be ranked from highest to lowest as follows: (1) GFR, (2) LFR and LSFR, and (3) SFR. Both the lead- and salt-cooled designs achieve about 30% higher power density than the gas-cooled reactor, but attain power density 3 times smaller than that of the sodium-cooled reactor. Fuel cycle costs are favored for the sodium reactor by virtue of its high specific power of 65 kW/kgHM compared to the lead, salt and gas reactor values of 45, 35, and 21 kW/kgHM, respectively. In terms of safety, all concepts can be designed to accommodate the unprotected limiting accidents through passive means in a self-controllable manner. However, it does not seem to be a preferable option for the GFR where the active or semi-passive approach will likely result in a more economic and reliable plant. Lead coolant with its superior neutronic characteristics and the smallest coolant temperature reactivity coefficient is easiest to design for self-controllability, while the LSFR requires special reactivity devices to overcome its large positive coolant temperature coefficient. The GFR required a special core design using BeO diluent and a supercritical CO_2 reflector to achieve negative coolant void worth—one of the conditions necessary for inherent shutdown following large LOCA. Protected accidents need to be given special attention in the LSFR and LFR due to the small margin to freezing of their coolants, and to a lesser extent in the SFR.

1. Introduction

Fast reactors can be designed with various coolants. The coolants that were principally explored during the early days of atomic energy included sodium, lead–bismuth, and helium. The coolant for fast reactors was universally chosen at that time to be sodium. This is because the main mission of fast reactors was to breed more fuel as fast as possible, thus achieving the minimum doubling time, i.e., the time it takes the breeder to double its fuel. To accomplish this goal, the core design needed to have very high power density. Sodium coolant with its superior heat transport characteristics and excellent neutronic properties, in addition to its good compatibility with structural materials, became clearly the most suitable candidate of choice.

With the arrival of the Generation IV program (GIF, 2002), which selected lead-alloy and gas-cooled fast reactors for future evaluation and development, interest in alternative coolants to sodium was renewed. The question that readily arises is why, then, this new interest in new coolants given the fact that sodium superiority had been established, given significant R&D expenditures associated with development of databases for new coolants? The major reason is that the mission of fast reactors has shifted from that of the minimization of doubling time to broader objectives, as given by Generation IV goals. These include, among other objectives, waste management as part of a sustainability goal in addition to the traditional emphasis on resource utilization. Therefore, transmutation of nuclear waste has become a new mission for fast reactors. Concurrently, economic competitiveness of new reactors has become a key target to be addressed, since without the ability to compete in the deregulated marketplace, the other objectives become moot. Because the early sodium-cooled reactors were more expensive than light water reactors (LWRs) due to their more complex design, that requires an additional heat transport system to mitigate consequences of sodium chemical reaction with water/steam/air, measures addressing sodium fires and its high Na-24 isotope activity, as well as more complex maintenance and refueling because of sodium opacity, there is motivation to evaluate alternative coolants if they could afford simplification of the design and potential cost

* Corresponding author.
E-mail address: hejzlar@mit.edu (P. Hejzlar).

0029-5493/$ – see front matter © 2009 Elsevier B.V. All rights reserved.
doi:10.1016/j.nucengdes.2009.07.007

Nomenclature

A	flow area (m^2)
c_p	specific heat (J/(kg K))
D	diameter (m)
D_h	hydraulic diameter (m)
k	thermal conductivity (W/(m K))
$\dot{m}$	mass flow rate (kg/s)
Nu	Nusselt number
P	pitch (m)
Pr	Prandtl number
Re	Reynolds number
Δp	pressure drop (Pa)
$\dot{Q}$	heat rate (W)
T	temperature (K)
V	velocity (m/s)

Greek symbols

β	coefficient of thermal expansion (1/K)
μ	dynamic viscosity (kg/(m s))
ρ	density (kg/m^3)

Subscripts

In	inlet
Out	outlet

reduction. Moreover, sodium has a relatively low boiling point, limiting core outlet temperatures to values that are not overly attractive for the flexible mission of both electricity production and liquid fuel (e.g., hydrogen) production. Reflecting this expansion of fast reactor mission and in an effort to address the broad Generation IV goals, new coolants and their potential to enhance performance of fast reactors for the 21st century deserve a renewed look.

This paper utilizes the opportunity of completion of three conceptual reactor designs at MIT within the framework of two nuclear research energy initiative (NERI) projects to compare these reactor concepts, optimized for various coolants, with a sodium-cooled reactor. The alternative coolants are lead, which has recently received extensive study (Adamov et al., 1997; Todreas et al., 2004), but also new coolants that have not been looked at before—ternary chloride liquid salt and supercritical carbon dioxide (S-CO_2). The liquid salt was selected because it is optically transparent making inspection and maintenance much easier than for opaque coolants, such as sodium or lead. Although there are many possible liquid salt candidates, only the ternary chloride liquid salt, NaCl–KCl–$MgCl_2$ (30–20–50), is included in this inter-coolant comparison. This is because extensive neutronic and thermal hydraulic evaluation of various salt candidates for application as a fast reactor coolant, documented in accompanying papers (Petroski et al., 2009; Shwageraus and Hejzlar, 2009), showed this salt to be the best candidate. Therefore, only the best performing salt among liquid salt alternatives is included in this coolant comparison. Supercritical CO_2 was selected because it offers, in the direct cycle gas-cooled fast reactor (GFR) configuration, an attractively high plant efficiency at moderate temperatures compatible with structural materials and high compactness of power conversion system. This high efficiency is expected to reduce cost.

Comparison of coolants for fast reactors can be found in a number of nuclear engineering books and papers. Educational materials typically focus on comparison of advantages and drawbacks of property values. Among more recent works going beyond the simple evaluations-based properties, an excellent comparison of sodium against heavy liquid metal coolants was given in Spencer (2000), who compares key properties of individual coolants, neutronic and thermal hydraulic performance advantages and drawbacks, including compatibility with structural materials and other considerations. Ninokata et al. (2000) expands the comparison of sodium and lead alloy coolants by including safety aspects. In this paper, the properties will be summarized briefly in the next section to include the two new coolants that were not explored in earlier literature. However, the major focus of the comparison will be on the impact of coolant properties on fast reactor designs. The unique opportunity offered by this project is that the four fast reactor concepts compared here were developed with the same Generation IV goals in mind; all can withstand unprotected accidents and have the same power rating. For some designs significant effort was required to overcome physical property limitations to achieve desirable goals. Therefore, the focus of this comparison will be on the implications of coolant properties on fast reactor designs, figures of merit for optimized designs and design choices which alleviate property constraints.

2. Brief comparison of key coolant properties

Table 1 compares thermophysical properties of the four coolants considered: lead, sodium, liquid salt NaCl–KCl–$MgCl_2$ (30–20–50), and supercritical carbon dioxide. The properties are presented for two temperatures: 450 °C—a typical core inlet or average temperature during steady state, and 700 °C, which represents an expected temperature during transients. Liquid metals are an attractive coolant choice because they have good heat transfer properties and no need for pressurization. In particular, sodium thermal conductivity is nearly four times higher than that of lead, resulting in smaller values of film temperatures. Gases and liquid salt coolants are non-corrosive, transparent and do not react with secondary fluids or air.

To a large extent, the melting and boiling temperatures of coolants define the operating temperature window of the reactor systems. The boiling temperatures for all liquid coolants are well beyond the cladding failure limits. In addition, due to the high boiling temperatures of salt and lead coolants, certain problems such as coolant voiding due to boiling in the core and associated reactivity insertion during accidents are effectively eliminated. Sodium has the lowest boiling temperature among all coolants, which raises safety concerns during accidents involving substantial coolant heatup. Conversely, the melting temperatures of salt and lead are relatively high compared to sodium, which creates additional operational constraints on reactor temperature during transients and refueling to avoid freezing. These boiling or freezing concerns are eliminated for gas-cooled reactors. However, gas reactors must be kept at high pressure to achieve an acceptably high heat transfer rate and, in the case of the direct S-CO_2 cycle, to take advantage of reduced pumping power near the critical point. This raises challenges for the design of GFR post-LOCA decay heat removal systems, since heat removal capacities of gases at low pressure are mediocre.

Sodium coolant requires tight core packing because of neutronic reasons. A small coolant fraction is possible due to the low viscosity of sodium, which yields acceptable pressure drop and pumping power. On the other hand, the higher viscosity of lead and its very high density require a looser lattice to keep pressure drop and pumping power within acceptable limits. Although this is neutronically possible due to the low moderating power of lead, as a result lead cores achieve significantly lower power densities than sodium-cooled cores.

In the case of salt-cooled reactors, coolant density is comparable to sodium, but viscosity is much larger than both sodium and lead. Contrary to lead coolant, liquid salt coolants cannot employ a more open lattice because of the appreciable moderating power and large thermal expansion coefficient of liquid salts, which would result in unacceptably high coolant temperature reactivity coeffi-

Table 1
Key thermophysical and neutronic properties of coolants.

	Lead[a]	Sodium[a]	Salt NaCl–KCl–$MgCl_2$ (30–20–50)	S-CO_2[b] at 20 MPa
Boiling point (°C)	1737	892	2500	−78
Melting point (°C)	327.4	97.8	396	−58
Density, ρ (kg/m^3)				
At 450 °C	10,536	842	1910	143.75
At 700 °C	10,242	780	1715	104.16
Thermal expansion coefficient, α (% Vol/K)				
At 450 °C	0.011	0.029	0.041	0.152
At 700 °C	0.012	0.031	0.045	0.104
Dynamic viscosity, μ (kg/(m s))				
At 450 °C	2.01×10^{-3}	2.59×10^{-4}	3.47×10^{-3}	3.46×10^{-5}
At 700 °C	1.40×10^{-3}	1.81×10^{-4}	1.18×10^{-3}	4.17×10^{-5}
Thermal conductivity, k, (W/(m K))				
At 450 °C	15.4	66.1	~0.39	0.056
At 700 °C	17.7	59.1	~0.39	0.072
Specific heat, c_p (J/(kg K))				
At 450 °C	147	1272	~1004.	1227.0
At 700 °C	147	1276	~1004.	1267.9
Density-specific heat product, ρc_p (J/(cm^3 K))				
At 450 °C	1.55	1.07	1.92	0.18
At 700 °C	1.51	1.00	1.72	0.13
Pr number				
At 450 °C	0.0192	0.0050	8.9330	0.7581
At 700 °C	0.0116	0.0039	3.0377	0.7343
Macroscopic capture cross-section relative to sodium[c]	6	1	22	0.2
Moderating power ($\xi\Sigma_s$)[c]	0.0024	0.0078	0.0073	0.0025
Moderating ratio ($\xi\Sigma_s/\Sigma_a$)[c]	19	370	16	525
Transparency	Opaque	Opaque	Transparent	Transparent

[a] Kutateladze et al., Liquid Metal Coolants, Atomisdat, Moscow, 1976.
[b] NIST Website: www.nist.org.
[c] Calculated for spectrum specific to each reactor type.

cients. Therefore, liquid salt-cooled cores require a tight core lattice. Further, the thermal conductivity of salts is very small, resulting in a large film temperature drop, which is further exacerbated by the effect of high viscosity, and thus low Reynolds number. Therefore, the achievable power density of the salt-cooled cores will be limited in spite of their tight lattice geometry. On the other hand, because of their high heat capacity relative to sodium, salt coolants can store large amounts of decay heat during transients, making them attractive from a safety point of view.

S-CO_2 gas is a poor heat transfer fluid compared to the other coolants because of its low density at comparable low operating pressure. To overcome the negative effects of this low density, the gas must be pressurized. The very small thermal conductivity of S-CO_2 results in much smaller heat transfer coefficients than for liquid metals. Also, heat transport capacity is small because of the very small density-specific heat product, resulting in a need for high flow rates, and thus high pumping power. This becomes especially challenging in case of a loss of coolant accident when gas density is significantly reduced and heat transport capacity becomes mediocre.

Regarding the neutronic properties, neutron capture and moderating power are of interest. For fast reactors, small macroscopic capture cross-section and small moderating power are desirable. Examining these data in Table 1, which were generated in spectra specific to central core regions of each reactor type and for typical coolant conditions, one can observe that salt and sodium have comparable moderating power, about 3 times larger than that of lead or S-CO_2. Salt has also the largest macroscopic cross-section (22 times larger than sodium). Thus, salt is neutronically the most challenging coolant for fast reactor design. The comparison of moderating ratio shows some surprising observations. First, the salt coolant, which consists of relatively light nuclei, has the smallest moderating ratio; by an order of magnitude smaller than that of sodium. This is because the most abundant Cl35 has a small scattering cross-section in a fast spectrum and because salt has the largest absorption cross-sections among these four coolants. Even more surprising is the high moderating ratio of supercritical CO_2—a consequence of the high scattering cross-section of carbon and small macroscopic absorption cross-section of CO_2.

3. Representative conceptual designs and their descriptions

Specific reactor designs selected for the comparison are all power reactors of the same rating—2400 MWt. The designs to be compared are:

1. A gas-cooled fast reactor (GFR) with unity conversion ratio developed at MIT under a NERI project (Handwerk et al., 2006, 2007).
2. An uprated version of a sodium-cooled actinide burning reactor (ABR), designated SFR in this paper, based on an ANL 1000 MWt design (Hoffman et al., 2006).
3. A lead-cooled fast reactor with flexible conversion ratio (LFR), developed in this project and described in an accompanying paper (Nikiforova et al., 2009).
4. A liquid salt-cooled reactor with flexible conversion ratio (LSFR), developed in this project and described in accompanying papers by Petroski et al. (2009) and Shwageraus and Hejzlar (2009).

Although two 2400 MWt GFR designs are under development, the Commissariat à l'Energie Atomique (CEA) helium-cooled GFR concept and the MIT S-CO_2-cooled concept reactor, only the latter will be used for comparison since its data are more readily available and the same neutronic analysis methods and libraries were used for its design as for the lead and liquid salt concepts. For the SFR con-

Table 2
Main characteristics of fast reactor concepts to be compared.

	GFR	SFR	LFR	LSFR
Operating characteristics				
Power rating (MWt)	2400	2400	2400	2400
Power density (kW/l)	85.4	290	112	130
Cycle length (years)	18	3.5	5.4	5.8
Batch management	1 batch	1 batch	1 batch	1 batch
Coolant parameters				
Coolant	S-CO_2	Sodium	Lead	NaCl–KCl–$MgCl_2$ salt
Primary system pressure (MPa)	20	0.1	0.1	0.1
Core inlet temperature (°C)	485.5	371	479	496
Core outlet temperature (°C)	650	510	573	581
Core flow rate (kg/s)	11,708	13,580	173,600	29,000
Fuel and its characteristics				
Fuel	(U–TRU–Be)O_2	U–TRU–Zr	U–TRU–Zr	U–TRU–Zr
TRU enrichment (wt%)	16.6%	15.2%	16.7%	15.7%
Discharge burnup (MWd/kg)	140	72	77	67
Specific power (kW/kg)	20.7	64.8	44.7	35.0
Radial power peaking	1.3	1.22	1.21	1.3
Geometry and dimensions				
Lattice type	TID[a]/HEX	Pin/HEX	Pin/Square	Pin/HEX
Lattice P/D	1.59	1.08	1.3	1.19
Core active height (m)	1.54	1.02	1.3	1.3
Equivalent core diameter (m)	4.8	3.2	4.6	4.25
Active core volume (m^3)	27.9	8.7	21.5	18.5
Vessel outer diameter (m)	11.5[b]	10.2	10.2	10.2
Number of assemblies	397	360	349	451
Number of pins per assembly	265[a]	271	441/416	390/372
Other				
Cladding	ODS steel	HT-9	T-91	T-91
Peak cladding temperature (°C)	810	550[a]	614	650
Decay heat removal	Active/passive[c]	Passive RVACS	Passive RVACS + ACS[d]	Passive RVACS + ACS[d]
Power conversion system	Direct S-CO_2	Rankine/S-CO_2	Indirect S-CO_2	Indirect S-CO_2
Reactor vessel	PCIV[b]	Pool type	Pool type	Pool type

[a] Tube-in-duct design with coolant inside the tubes and fuel outside, therefore number of coolant holes is reported instead of number of pins for TID.
[b] Pre-stressed cast iron vessel (PCIV).
[c] Active with blowers backed up by natural circulation of CO_2 at elevated containment pressure.
[d] Enhanced RVACS using dimples and perforated plate plus passive secondary auxiliary cooling system via natural circulation of CO_2 through IHX to HX in the in-containment water storage tank.

cept, a metallic[1] fueled core was selected for consistency with the lead- and salt-cooled fuel. The metallic fueled SFR concepts available are rated at 1000 MWt (S-PRISM, ABR1000). For consistency, the 1000 MWt ABR concept developed at ANL (Hoffman et al., 2006) was taken as a starting point and the number of core assemblies was increased to achieve the 2400 MWt power rating. Further, the number of batches was changed from 3 to 1 and Zr weight fraction grading rather than enrichment grading was used, as for the LFR and LSFR cores. Full neutronic analysis of the 2400 MWt SFR core was performed to obtain reactivity coefficients, power distribution and heavy metal mass balances. Core thermal hydraulics will be similar to the original ABR core because core temperature rise is preserved, core peaking is smaller than in the original design, and flow rate per fuel assembly is also preserved. SFR transient analyses including plant and decay heat removal (DHR) system design were beyond the scope of this project. However, it is assumed that adequate DHR systems, using either the enhanced reactor vessel auxiliary cooling system (RVACS) supplemented by a passive secondary auxiliary cooling system (PSACS) described in an accompanying paper (Todreas et al., 2009) or a direct reactor auxiliary cooling system (DRACS), can be developed for the SFR. Because the GFR is designed only for unity conversion ratio (CR = 1), the comparison will focus on the unity conversion ratio cases.

A general comparison of key reactor characteristics is provided in Table 2. Since the sodium-cooled SFR and GFR are not part of this project versus the LFR and LSFR, which were described in detail in accompanying papers (Nikiforova et al., 2009; Petroski et al., 2009), Sections 3.1 and 3.2 will provide brief descriptions of the GFR and the SFR, respectively.

3.1. Gas-cooled fast reactor brief description

The overall layout of the GFR plant is shown in Fig. 1. The reactor core is cooled by S-CO_2 at a pressure of 20 MPa directly coupled to a S-CO_2 power cycle. The choice of direct cycle is based on economics; the thermodynamic efficiency gained by using a direct cycle versus a gas-to-gas indirect cycle is about 2%, and the capital cost is also reduced by eliminating the need for heat exchange to secondary loops. Heat is removed by four power conversion system (PCS) loops rated at 300 MWe each. The design employs a PCS horizontal layout and has the same arrangement as shown in the lead paper of this special issue (Todreas et al., 2009). Having four PCS loops versus one allows individual loops to be isolated for maintenance, leak isolation, and part-load operations while maintaining high thermal efficiency. Each PCS module utilizes the Brayton recompression cycle with minimum and maximum temperatures of 32 and 650 °C,

[1] Although there are other fuel forms that could be used with most reactor concepts under investigation in this project, such as oxide or carbide fuels, which are currently under study in the French SFR program (Buiron et al., 2007), or nitride fuels explored in Russia for LFR (Adamov et al., 1997), metallic fuel has been chosen for consistency for all reactor concepts except for the GFR, where metal fuel is not feasible due to its low fuel melting point. The major motivation for metal fuel selection was its superior performance in unprotected transients since achievement of inherent shutdown in accidents with failure to scram was one of the major design goals. Other fuel forms could be also potentially used, but were not investigated in this project.

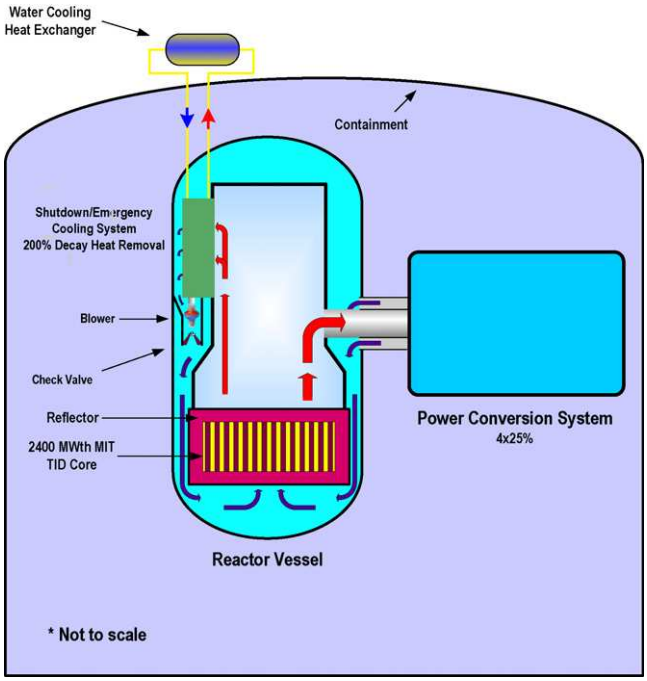

Fig. 1. Schematic layout of GFR plant with active SCS/ECS.

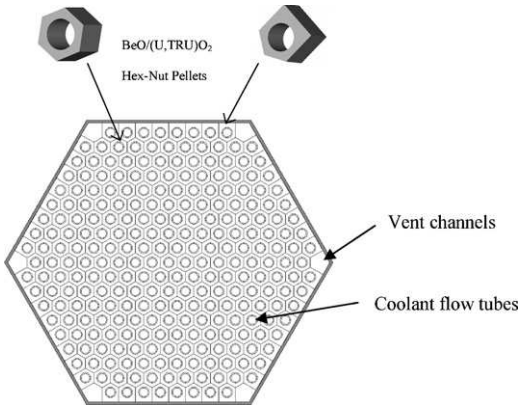

Fig. 2. Horizontal cross-section view of TID fuel assembly.

respectively. Peak and minimum pressures in the system are 20 and 7.69 MPa, respectively.

The GFR has a conversion ratio of unity and does not use any blankets, for enhanced proliferation resistance. In the absence of blankets, a high fuel volume fraction (hence low coolant volume fraction) is necessary to boost the core conversion ratio and reactivity-limited burnup. The requirement for low coolant void reactivity also requires small coolant fraction. Furthermore, the requirement of fuel chemical stability with the S-CO_2 coolant requires the use of oxide fuel, which has a relatively low heavy metal density and thus favors a high fuel volume fraction in the core. To satisfy these requirements, a low coolant volume fraction of 25% is used.

If fuel were arranged in a hexagonal array of pins packed tightly enough to have 25% coolant by volume, the resulting small hydraulic diameter would cause an unacceptably high core pressure drop. A fuel pin arrangement was thus discarded in favor of "inverted" fuel geometry similar to the prismatic block-type fuel found in a VHTR. In order to achieve high fuel volume fraction with inverted-geometry fuel elements which would not be corroded excessively by high-temperature CO_2 and maintain structural integrity with burnup, a vented fuel assembly design was conceptualized. This tube-in-duct (TID) fuel assembly consists of a hexagonal duct with internal coolant flow tubes inside. Fuel is placed around coolant tubes and inside the hexagonal duct. To keep stresses on the duct wall acceptable and to minimize duct thickness, the TID fuel assembly is vented. Fig. 2 shows a horizontal cross-sectional view of a TID fuel assembly. Table 2 gives a high discharged burnup of 140 MWd/kg. Although this burnup is achievable in terms of neutronic considerations, it is quite high for oxide fuel and the ability of the proposed TID oxide–BeO fuel to achieve these high burnups needs to be confirmed by further R&D programs. Further detail on the conceptual design of the TID assemblies is provided in Handwerk et al. (2006) and Pope et al. (2003).

Beryllium oxide (BeO) is specified for use as a diluent in the fuel for a number of reasons. If (U,TRU)O_2 fuel were to be used without this diluent, the reactor would exhibit a positive coolant void reactivity in excess of $1. The radial power shape without diluent would change dramatically during a cycle and the reactivity swing would be very large, requiring a large number of high-worth control rods. It has been shown that the addition of BeO to the fuel matrix reduces coolant void reactivity and provides the means to flatten the radial power over a very long cycle. BeO also increases the critical enrichment, which can lower the conversion ratio to just above unity, giving a relatively flat reactivity during the core life and also reducing the reactivity hold-down burden on the control rods (Handwerk et al., 2006). With an unusually high thermal conductivity for an oxide, BeO also has been shown to significantly augment the thermal conductivity of UO_2 pellets. The core employs 3 rows of S-CO_2 reflectors—highly orificed ducted subassemblies with no internal structures and full of CO_2 coolant, which escapes upon loss of pressure, enhancing neutron leakage (see Handwerk et al., 2007 for more details). This reflector, together with the BeO diluent effect on neutron spectrum, yields negative coolant void reactivity—a unique achievement in large fast reactor cores.

In Fig. 1, the basic arrangement of the shutdown/emergency cooling system (SCS/ECS) is depicted. This system consists of four sets of CO_2-to-water heat exchangers attached to the upper portion of the reactor barrel. There are four separate loops, each capable of removing 50% of the decay heat. This $4 \times 50\%$ arrangement forms a 2-out-of-4 system where one SCS/ECS module (or loop) can be out of service for maintenance and a second loop can fail, and sufficient decay heat removal is still provided by the two operational loops. This provides highly reliable decay heat removal in shutdown and postulated accident conditions.

In normal operation, the check valves are held shut by the core pressure drop, and S-CO_2 in the SCS/ECS modules is nearly stagnant. During shutdown or emergency cooling, the check valves open, allowing CO_2 to leave the upper part of the chimney and enter the printed circuit heat exchanger (PCHE) hot side, where it is cooled by a water loop. After leaving the heat exchanger, the CO_2 is circulated by blowers through the open check valves and would then return to the vessel downcomer. The water loop transfers heat from the CO_2-to-water heat exchangers and then to a water/water heat exchanger submerged in a spray pond (as the ultimate heat sink) located outside of the containment.

Although it is possible to design a S-CO_2-cooled GFR that can survive LOCA by cooling the core through naturally circulating loops between the core and elevated emergency cooling heat exchangers, it is not an attractive approach because of various bypass paths that can, depending on break location, degrade core cooling. Moreover, natural circulation gas loops can operate in deteriorated heat transfer regimes with a substantial reduction of the heat transfer coefficient – as low as 30% of forced convection values – and data and correlations in these regimes carry large uncertainties (Lee et al., 2008). Therefore, reliable battery powered blowers for post-

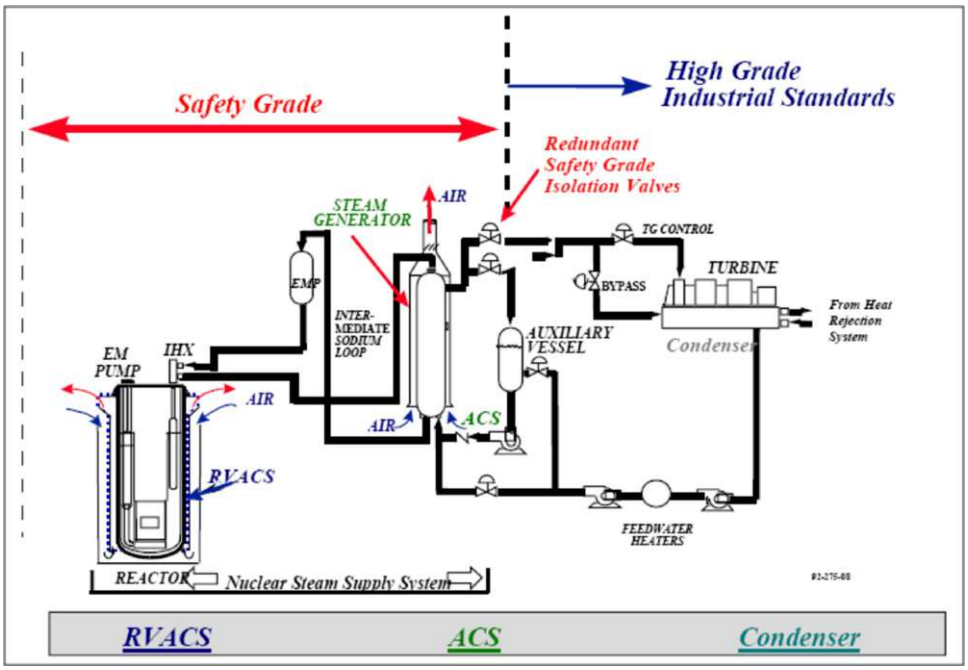

Fig. 3. Schematic of main power train and heat removal for S-PRISM (from Boardman et al., 2000).

LOCA decay heat removal (DHR) were selected which provide flow in well defined regimes with low uncertainty and can be easily overdesigned to accommodate bypass flows. The results confirmed that a GFR with such a DHR system and negative coolant void worth can withstand a LOCA with and without scram as well as loss of electrical load without exceeding core temperature and turbomachinery overspeed limits.

3.2. Sodium-cooled fast reactor brief description

The design of the sodium-cooled 2400 MWt reactor plant is beyond the scope of this project. Hence, the 2400 MWt sodium-cooled plant sizing and layout was not carried out except for the conceptual core design. The core configuration is based on an ANL 1000 MWt metallic fueled core design (Hoffman et al., 2006). It employs 360 hexagonal assemblies, each having 271 fuel pins with the total number of fuel pins in the core significantly smaller than the salt- or lead-cooled designs. The pressure drop through the active core is relatively small, on the order of 0.2 MPa. The operating temperatures were calculated for a typical sodium core design, but with the development of advanced materials for cladding and structural components there is the potential to raise the operating temperatures and achieve higher plant efficiency[2]. A detailed description of the sodium core neutronic design and thermal hydraulic subchannel analysis performed in this project is provided in Todreas et al. (2008).

The ANL design is based on the S-PRISM 1000 MWt design, which is described in Boardman et al. (2000). Fig. 3 shows the schematic of the S-PRISM with main power train and heat removal systems. It employs a safety grade auxiliary cooling system (ACS) via natural circulation of air past the shell of the steam generator and safety-grade RVACS to cool the reactor vessel assembly as decay heat removal systems. One main difference between the salt/lead and sodium reactors is the chemical reaction of sodium with water, air, and CO_2 gas. Therefore, S-PRISM, as well as most sodium reactors, uses an intermediate cooling loop in order to avoid the consequences of such reactions in the primary system as well as steam ingress into the core.

There are two key questions that remain unanswered:

1. Can a sodium plant be designed in a more compact configuration coupled to the S-CO_2 power cycle similar to that for lead/salt-cooled designs in this project? Since CO_2 also reacts with sodium, although at a slower rate than water, and does not produce hydrogen, the sodium/CO_2 IHX would have to be designed with double walls with helium detection for leaks in between the walls. Double wall steam generators were developed in Japan (Kubo et al., 1997), and Westinghouse and Toshiba proposed such steam generators for their actinide recycling reactor for the GNEP program (Energy Solutions, 2008). Therefore, it is not out of the question to consider the placement of IHXs in the annular space between the core barrel and the vessel liner in a similar manner as for lead and salt designs. The double-free-level reactor vessel design as proposed in this project would also eliminate the potential of high pressure gas ingress into the core. The feasibility of fitting four 600 MWt double-wall IHXs into a sodium vessel of 10.2 m would have to be confirmed. However, because the helium gap is 7 μm, yielding an effective thermal conductivity of the gap plus outer wall of 24 W/mK per the experimental measurements of Kubo et al. (1997), the double-wall design does not require a large increase of IHX volume. This increase can be compensated by the much higher sodium conductivity compared to lead or salt and the increased space available due to the smaller sodium-cooled core. Hence, it is expected that placement of sodium/CO_2 IHXs in the 2400 MWt vessel will be feasible.
2. Can a 2400 MWt core be cooled by passive decay heat removal means? Use of an enhanced RVACS as in the lead- and salt-cooled reactors could also be adopted for the sodium-cooled reactor. The PSACS design coupling the primary coolant to PSACS water tanks via a double-wall IHX can also be used. Overall, if the double-

[2] The SFR coolant outlet temperature is lower than that of the LFR or LSFR even though the cladding temperature limit is the same. This is because SFR design development was not part of this project and the SFR reactor design was taken from ANL work, based on an earlier S-PRISM design, which favored larger margins to material limits. We believe that higher core outlet temperatures are possible for the metallic-fueled SFR.

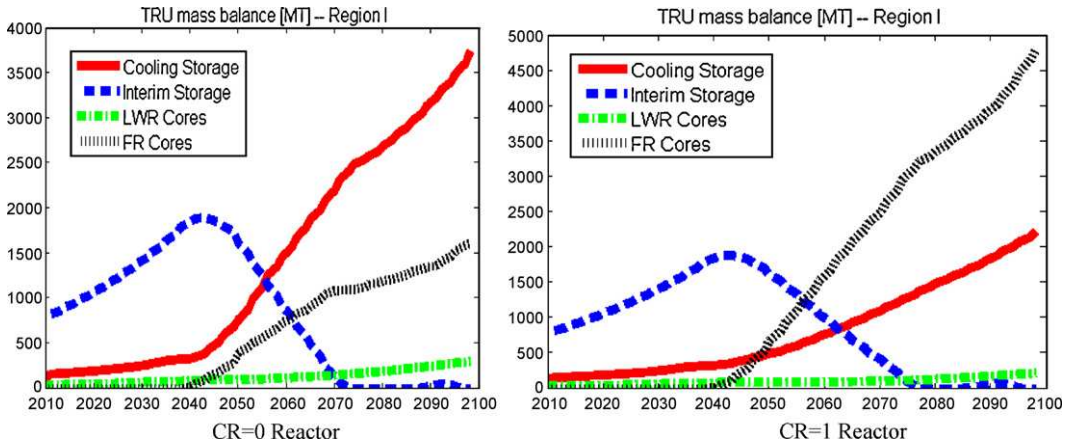

Fig. 4. Comparison of U.S. TRU inventories for recycling in CR = 0 and CR = 1 reactors (from Aquien et al., 2006).

wall IHX can be proven reliable, it is expected that the proposed RVACS/PSACS approach could also be used for passive decay heat removal for the 2400 MWt sodium-cooled reactor. Alternatively, DRACS can be utilized to supplement RVACS.

4. Comparison goals and overall results

The Generation IV Roadmap established design goals that future reactor designs should strive to achieve (GIF, 2002). These goals involve:

- *Sustainability*—"Generation IV nuclear energy systems will provide sustainable energy generation that meets clean air objectives and promotes long-term availability of systems and effective fuel utilization for worldwide energy production. Generation IV nuclear energy systems will also minimize and manage their nuclear waste and notably reduce the long-term stewardship burden, thereby improving protection for the public health and the environment."
- *Safety and reliability*—"Generation IV nuclear energy systems operations will excel in safety and reliability and will have a very low likelihood and degree of reactor core damage during any possible accident."
- *Economics*—"Generation IV nuclear energy systems will have a clear life-cycle cost advantage over other energy sources and will have a level of financial risk comparable to other energy projects."
- *Proliferation resistance and physical security*—"Generation IV nuclear energy systems will increase the assurance that they are a very unattractive and the least desirable route for diversion or theft of weapons-usable materials, and provide increased physical protection against acts of terrorism."

Regarding the proliferation goal, all fast reactors considered in this comparison do not use separated plutonium and do not employ blankets to avoid high-grade plutonium generation in the fuel. In fact, the conceptual design of these reactors has been carried out with these goals embedded in the process. As discussed in Section 5, neutron spectra among the different cores are also similar. Hence the plutonium isotopic vectors in the spent FR fuel will also be similar. Therefore, all designs of the same conversion ratio will have similar intrinsic proliferation resistance characteristics: the differences will stem from protective measures implemented throughout the entire fuel cycle, which is beyond the scope of this project.

Within this broad set of goals, our comparison will focus primarily on sustainability, economics and safety. This is because all the four systems to be compared within this project are fast reactors, all of which rank high for the sustainability goal since their CR = 1 cores have high uranium resource utilization and can not only manage their own nuclear waste but also reduce the long-term stewardship burden by depleting legacy TRU from spent LWR fuel. Nevertheless, we would like to point out some important aspects regarding sustainability.

4.1. Sustainability

We will focus our comparison regarding sustainability on the CR = 1 and CR = 0 core performance since all reactor concepts having unity conversion ratio have a similar performance in this respect.

First, it may be surprising that both the CR = 0 and CR = 1 cores can reduce the stockpile of spent LWR fuel at about the same time, although a smaller number of CR = 0 reactors would be needed. Fig. 4 plots the distribution of TRU inventories in the U.S. over the next hundred years and under the assumption of nuclear energy growing at a 2.4% annual rate, assuming that reprocessing plants and fast reactors become available by 2040. The results were obtained using the system simulation code developed at MIT, CAFCA II (Aquien et al., 2006). In Fig. 4, cooling storage curves depict TRU undergoing cooling in spent fuel pools of both LWRs and FRs, interim storage signifies TRU that is cooled enough and thus available for reprocessing, and LWR cores and FR cores show the inventory of TRU in the LWRs cores and FR cores, respectively. In spite of the fact that the net TRU destruction in the CR = 1 core is zero while CR = 0 is a pure TRU burner, both the CR = 0 and CR = 1 strategies deplete the legacy TRU at about 2070. This is because electricity growth demand is assumed to be preferentially satisfied by the fast reactor buildup if TRU is available, and new fast reactors require significant TRU loading for their first cores. As a result the TRU legacy is depleted and the construction rate of new fast reactors is limited after 2070 to available TRUs. The main difference between the CR = 0 and CR = 1 core designs is in the number of fast reactors that need to be built to produce the TRU distribution curves in Fig. 4—150 1000 MWe CR = 1 reactors versus 23 1000 MWe CR = 0 reactors would be operating by 2070.

Secondly, the CR = 1 cores use uranium resources much more effectively than the CR = 0 cores. Since CR = 1 cores manage the uranium resources more efficiently than CR = 0 cores and can still manage legacy TRU, they rank higher than the CR = 0 cores in the sustainability goal. However, because a large number of either CR = 1 or CR = 0 reactors is needed to accomplish TRU management, it is critical that their cost becomes competitive with that of LWRs in order to be preferred by utilities. Hence, attractive fast reactor economics needs to be a major effort in the design of future fast reactor systems. In this aspect, CR = 1 reactors have a better chance to be less costly because CR = 0 cores require a large number of con-

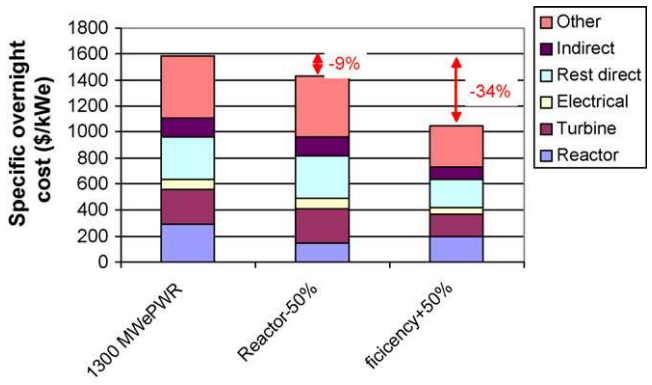

Fig. 5. Capital cost investment decomposition for typical evolutionary ALWR (from Hejzlar et al., 2006, data from OECD, 2000).

trol rods and their frequent replacement as well as a shorter cycle length that will reduce plant capacity factor.

4.2. Economics

If fast reactors are to make a significant impact on energy generation, resource utilization, and TRU management to reduce long-lived waste sent to a repository, large-scale deployment of fast reactors will be needed in the future, as was also revealed by the system-wide CAFCA II simulation above. This will be possible only if these reactors are economically attractive in comparison with LWRs and other power generation alternatives. Thus, in addition to excellent sustainability, substantial cost reduction becomes a major goal of future nuclear system development.

Today's capital investment to build a nuclear power plant is typically 60% of electricity generation cost, with fuel cost at 20% and operation and maintenance (O&M) cost incurring the remaining 20%. Since the capital investment cost constitutes the largest share of generation cost, its reduction is of prime interest for the Generation IV plants. The need to reduce capital cost of nuclear power plants has been recognized, and continuous effort has been directed at this objective for the last two decades. Measures include reliance on passive safety for emergency cooling, which allows reduction or elimination of complex and redundant safety grade equipment, design simplification, modularization, standardization, economy of scale and other approaches, as discussed in an OECD report (2000).

4.2.1. Economy of scale

One approach that has proven to reduce cost is economy of scale. Development of the Japanese sodium-cooled fast reactor (JFSR) design, with its thorough economic studies, has shown that an increase from 660 to 1500 MWe resulted in the largest reduction of cost per installed kWe among other approaches, which involved introduction of various innovative technologies and simplifications (Okada, 2008). Therefore, a large power rating of 2400 MWt was pursued for all fast reactor concepts in this project rather than small modular reactors. In this respect, all four reactor designs should benefit from economy of scale in the same manner.

4.2.2. Plant thermal efficiency

The second key factor affecting capital cost per installed kWe is plant thermal efficiency. Thus far, the major focus in the initiative for better economy of advanced nuclear power plants has been on the nuclear island, and a classical Rankine power cycle has been used as the balance of plant (BOP). However, the design improvements and simplifications of the nuclear island have only limited potential with respect to the reduction of capital cost, and thus generation cost. Fig. 5 (Hejzlar et al., 2006) shows the capital investment decomposition of a typical advanced LWR per data (since reliable commercial fast reactor data are not available) in an OECD report (2000). The direct costs include reactor plant equipment (designated "reactor" in Fig. 5) and turbine plant equipment (designated "turbine"), electrical plant equipment ("electrical") and the rest direct costs (land and land rights, main construction heat rejection system, and miscellaneous plant equipment and construction services). Indirect costs consist of design and engineering and project management. Finally, other costs involve owner's cost, spare parts, initial fuel costs, and contingencies.

In the leftmost column of Fig. 5, the reactor plant equipment clearly constitutes only a small fraction of the total specific overnight cost. Therefore, even large savings on the nuclear island through innovative designs cannot provide substantial reduction of specific cost, as shown on the middle column of Fig. 5, where one can observe that a 50% smaller cost of reactor plant equipment will lead to only 9% overnight cost reduction. However, advances in the power conversion system that achieve a higher plant thermal efficiency affect all components of the overall specific overnight cost. This is shown in the right column, where plant efficiency was increased by 50%, i.e., from the current 34% to 50%. Fig. 5 shows that a 50% efficiency increase can reduce specific overnight cost by 34%, which is nearly four times more than the 9% achieved by lowering the cost of reactor plant equipment by 50%. This is primarily because increased power cycle efficiency increases net electrical power and thus leads to a reduction of capital costs of all plant components, including indirect costs, on a per MWe basis. Therefore, if future fast reactors are to be highly competitive with LWRs and other electricity generating stations, the development of fast reactors must pursue higher plant thermal efficiency.

To increase plant efficiency, a number of design strategies can be used. The key strategies involve:

- Use of advanced materials having high allowable stresses and low creep at high temperatures, as well as good corrosion resistance.
- Maximization of core-average outlet temperatures through low radial peaking design and use of orificing.
- Minimization of temperature difference between the core outlet and turbine inlet by use of effective heat exchangers and minimization of heat transfer loops.
- Use of highly efficient advanced power conversion systems.

All of these approaches were used in the FCR design in this project. The higher the turbine inlet temperature, the higher is the efficiency. However, the achievable core outlet and turbine inlet temperatures are constrained by material limits. The core outlet temperature can be increased either by increasing the cladding steady state limit or by the reduction of film ΔT and making core outlet temperature more uniform. First, the cladding limit will be discussed, followed by approaches to reduce film ΔT and non-uniformities in core outlet temperature.

As discussed in the first accompanying paper (Todreas et al., 2009), T-91 with a steady state limit of 650 °C was selected as cladding material for the LFR and LSFR metal-fueled cores. Because lead corrosion at these temperatures is excessive, a corrosion resistant alloy cladding surface under development at MIT is required for the LFR to be able to operate with this temperature limit. The SFR uses traditional HT-9 steel for cladding, for which we assume the same limit. It is noted that low CR metallic fuel cores may require a lower limit because of the larger content of plutonium in the fuel, for which there are very limited data on Pu–Fe eutectic formation. However, should the irradiation data in the future show that eutectic formation is a problem, the potential cladding thinning from the eutectic can be overcome by the introduction of special foil liner between the cladding and the fuel that prevents Pu–Fe interaction. Additional R&D on this issue is more than worthwhile since the

economic benefit from increased efficiency will likely more than compensate for the expense.

Comparing the metal-fueled reactors with respect to the cladding temperature limit, the SFR, LFR and LSFR are assigned the same limit of 650 °C, with assumed modest advances in cladding material development and confirmatory testing. It is interesting to note that, although lead and salt have very high boiling points, which would allow them to operate at much higher temperatures than sodium (which boils at 883 °C), they cannot capitalize on this benefit due to the cladding limit, unless breakthrough advances in cladding materials are achieved. But even if such materials are available, the relatively low melting point of metallic fuel would become limiting. The GFR uses tube-in-duct oxide fuel with ODS cladding, which has a much higher temperature limit (800 °C). This is because a much higher clad limit than 650 °C was necessary due to the large film ΔT of gas. ODS (MA956) can accommodate this high temperature limit because (1) it has excellent creep resistance at high temperatures and (2) vented fuel is used, which does not expose cladding to stresses because of pressure differences across the cladding both during normal operation and during transients. Satisfactory performance of the selected ODS cladding at 800 °C during normal operation was confirmed by a Larson–Miller type analysis. On the other hand, the manufacturing of long ODS pins and their welding is a very difficult task that will require significant R&D and demonstration. Therefore, ODS was classified in the "stretch" category in the lead paper of this special issue (Todreas et al., 2009) as opposed to the "achievable" category for T-91. The use of ODS for metallic cores would not allow an increase of the cladding limit because of the eutectic Pu–Fe issue. If metallic fuel is replaced with oxide, it would be difficult to achieve the self-controllability due to relatively large Doppler feedback, as well as to design the CR = 1 core without blankets because of the low density of UO_2. Overall, the highest cladding steady state limit among the four evaluated reactors was the GFR, assuming that significant development and testing is successful, while all metal-fueled reactors are constrained by ~650 °C with no substantial potential for increase. A similar situation occurs with the transient cladding limit, which is significantly smaller for metal-fueled reactor concepts than for the oxide-fueled and ODS clad GFR.

The second strategy to maximize core outlet temperature is by pushing the core average outlet temperature as high as possible while satisfying the peak cladding limit. This can be done by minimizing film ΔT, minimizing radial peaking, and achieving an assembly flow distribution that well matches assembly power throughout irradiation. Film ΔT is proportional to heat flux and inversely proportional to heat transfer coefficient, which depends on coolant properties, flow and lattice geometry. Because the freedom to significantly vary the heat transfer surface in the core is limited, in particular for the CR = 1 core where high fuel volume fraction is required, it can be roughly stated that for fixed power density the larger the heat transfer coefficient, the smaller the film ΔT. Table 7 in Section 6 shows that the heat transfer coefficient of the SFR is 6.4 times larger than that of the LFR. The LFR's heat transfer coefficient is 5 times larger than that of the LSFR, and the LSFR is comparable to the GFR. The SFR is by far the clear winner in terms of a small film ΔT.

The non-uniform neutron flux in a reactor core results in core-wide power peaking. It is desirable to minimize this peaking and to achieve, as much as possible, a uniform core outlet temperature distribution. The typical strategy to minimize this peaking is through enrichment grading so that the zones with higher neutron flux have a lower content of fissile material than the zones with a lower neutron flux. In addition, fast reactors have canned fuel assemblies and use orificing to reduce flow in assemblies with lower power and force more flow into high-power assemblies. However, in fast reactors with a high conversion ratio, the bred-in plutonium in high flux regions moves the power profile back toward the fundamental mode during irradiation, making it difficult to keep a balanced power-to-flow ratio throughout the cycle using orificing. The innovative approach used here in all four fast reactor concepts differs in that it tailors a diluent content (zirconium in metal-fueled reactors and BeO in the GFR) in the radial fuel zones while keeping the TRU-to-uranium ratio constant. This yields low power peaking, which remains relatively constant throughout the cycle making it easier to orifice the assemblies and make core-outlet temperature more uniform. Because all four reactors use this approach, they can all benefit from an increased core-average temperature.

It is interesting to note that even though the heat transfer coefficient of the SFR is the largest; its core outlet temperature in Table 2 is the lowest (510 °C). However, this is most likely because core inlet and outlet temperatures were adopted from an earlier S-PRISM design, which used materials available in the 1990s and used internal and radial blankets and enrichment grading in the driver core. Hence peaking was larger than in the blanket-free designs with diluent grading. Moreover, S-PRISM went through a much more detailed design, incorporating engineering and hot channel factors, while the conceptual designs in our scoping study were not examined at this level of detail. Also, it is important to note that the sodium core has a three times greater power density than the other three cores. This requires larger margins to accommodate transients. It is expected that the sodium metallic core outlet temperature can be increased to about 550 °C, as suggested by Westinghouse/Shaw/Toshiba in a recent report on GNEP Deployment Studies for DOE (Energy Solutions, 2008). This would be much closer to the core outlet temperatures of lead- and salt-cooled reactors of 573 and 581 °C, respectively.

Minimization of the temperature difference between the core outlet and turbine inlet is accomplished in the LFR and LSFR by eliminating an intermediate loop, typically used for sodium-cooled reactors to transfer heat directly from the primary coolant to the power conversion system fluid via the IHX. This results in a turbine inlet temperature increase of 20–25 °C, achieving a turbine inlet temperature of 546 °C for both designs. This is possible because CO_2 does not react with lead or salt in case of an IHX leak or tube failure. The S-CO_2 direct cycle GFR is unique among the four contenders because the working fluid of the power cycle can also be used for core cooling in a direct cycle arrangement, eliminating the IHX altogether and achieving a turbine inlet temperature of 650 °C, by far the highest, translating to 47% plant efficiency compared to 44% for the LFR and LSFR. For the SFR, elimination of the intermediate loop is challenging because of the energetic reaction of sodium with water and hydrogen generation. This may be possible with the S-CO_2 power cycle since the reaction with CO_2 is slower and leaks may be preventable if a double-wall IHX with helium between the walls for leak detection is used. However, significant R&D is required to confirm the feasibility of this option. Overall, the potential to achieve the highest efficiency among the four reactor concepts can be ranked from highest to lowest as follows: (1) GFR, (2) LSFR and LFR, and (3) SFR.

Finally, the selection of power conversion system has key implications for plant efficiency. Four major power conversion system candidates that could be used in conjunction with most Generation IV concepts and achieve higher efficiency than LWRs with a classical Rankine cycle have been explored by Dostal et al. (2004). Their cycle efficiency as a function of turbine inlet temperature is plotted in Fig. 6. Note that both the superheated and supercritical steam cycles yield higher efficiencies than Brayton cycles at lower turbine inlet temperatures. However, their efficiency gain with temperature is small and at temperatures above 450 °C (superheated steam) and 550 °C (supercritical steam) they are outperformed by a supercritical CO_2 cycle. The helium Brayton cycle can achieve high efficiencies but requires high temperatures (800 °C and above). The S-CO_2 cycle

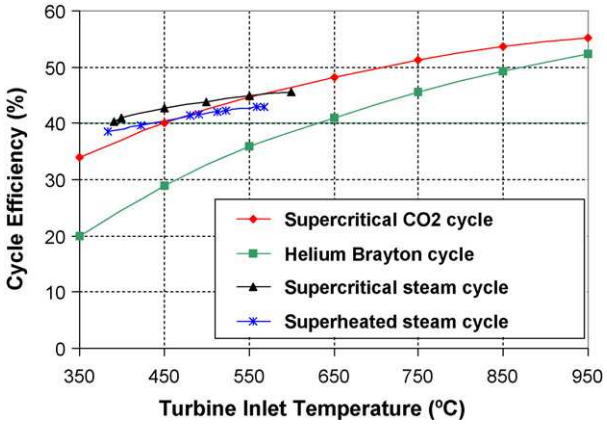

Fig. 6. Achievable efficiencies of various power cycles (from Dostal et al., 2004).

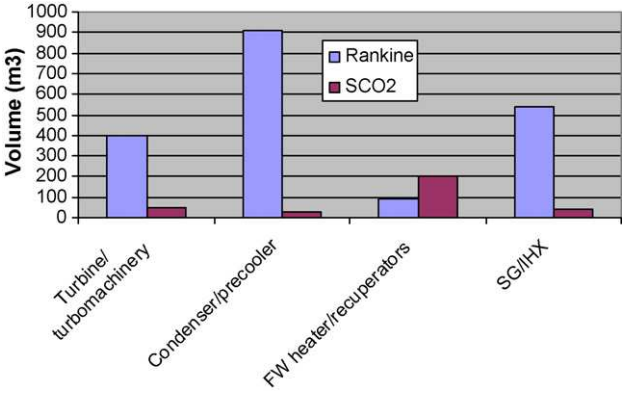

Fig. 7. Comparison of volumes of PCS components for 300 MWe S-CO_2 and Rankine cycles.

was selected as the PCS for all four reactors because it achieves higher efficiencies than a superheated steam cycle for turbine inlet temperatures above 450 °C, which are achievable for all the reactors compared, and because its efficiency gain at the higher temperature range is larger than that of the Rankine cycle. Also, this makes the plant comparison consistent, since each plant has the same power cycle. The supercritical steam cycle is also a strong contender that would deliver higher efficiency for the SFR, but it cannot be used for a direct cycle GFR. Also, supercritical water is very corrosive, and it may be difficult to design a reliable double-wall heat exchanger that would guarantee no leak into sodium.

Overall, all four reactors can use the S-CO_2 power cycle, but the reactor with the highest turbine inlet temperature (GFR) will benefit most in terms of efficiency. On the other hand, the SFR will benefit the least, and the efficiency gain compared to a Rankine cycle will be the smallest, depending on the possibility of eliminating the intermediate loop. However, if future R&D confirms that the CO_2/sodium reaction is slow and not a serious challenge, making it possible to use a sodium/CO_2 double wall IHX without the intermediate loop, the efficiency gain versus the Rankine cycle with intermediate loop will be significant.

4.2.3. Plant compactness

The capital cost to a large extent is proportional to the amount of steel and concrete consumed to build a new power plant. These two commodities form more than 95% of construction material inputs (Peterson, 2005) and have become increasingly more expensive because of the rapidly growing consumption of these materials in China and India. Furthermore, both these materials require a large amount of energy to produce and have appreciable carbon footprints such that any potential future carbon taxes will exacerbate their cost in a carbon-constrained economy. Therefore, plant designs with small volume and a small amount of concrete and steel used per installed MWe are expected to have a lower cost. Peterson (2005) compared the volumes of buildings, concrete, and steel needed to build various thermal reactors and showed that modular, low power density systems, such as the PBMR, require much larger volumes per MWe than PWRs. On the other hand, the thermal liquid salt intermediate temperature reactor AHTR, which has a large power rating and relies on inherent reactor shutdown and passive decay heat removal, was shown to have the lowest consumption of these materials. Although this is partly due to its significantly higher plant efficiency discussed earlier, it is evident that highly efficient, simple, and compact designs with large power rating have the potential to substantially reduce cost.

The lead- and salt-cooled fast reactors developed in this project have 10 times higher power density than the AHTR and about the same reactor vessel size but a much smaller guard vessel (10.2 m OD versus 16 m OD for the AHTR). Although the approach of decay heat removal for the AHTR is different, the nuclear island for the lead- and salt-cooled designs seems to be more compact than that of the AHTR. In addition, the S-CO_2 PCS is more compact and simpler than the multi-reheat helium Brayton cycle used in the AHTR. This is because the S-CO_2 cycle turbine outlet pressure of 7.7 MPa is just above the critical point, where the S-CO_2 density is very high, resulting in very compact turbomachinery and heat rejection heat exchanger. Moreover, it does not need any intercooling or reheat. For these reasons, compact designs of lead- and salt-cooled FCRs are expected to have steel and concrete volume savings at least comparable to those of the AHTR, which is expected to project to appreciable cost savings.

The compactness of the S-CO_2 cycle can be illustrated by a volume comparison against the Rankine power cycle, which has been used for all nuclear reactors up to date. Fig. 7 compares volumes of key components of Rankine and S-CO_2 power cycles for 300 MWe PWR plants. The very substantially smaller volume of the S-CO_2 PCS is clearly evident from this figure. The large turbine and condenser volumes of the Rankine cycle are consequences of the near-vacuum discharge pressure of steam turbines. The compactness of the S-CO_2 PCS was a major reason (in addition to its superior efficiency) for the selection of this cycle for the fast reactor concepts in this study.

The sodium core has the largest power density among all concepts (3 times more than the lead FCR) and thus the smallest core size. However, for the passive DHR configuration, relying on heat transfer through the vessel, large vessel size is preferred to maximize the decay heat removal rate. Thus, savings from a smaller vessel size cannot be realized. The benefit of a smaller core is more space to place pumps and other primary system components than in the LCR or LSFR. If the feasibility of a sodium reactor coupled to the S-CO_2 power cycle without an intermediate loop can be confirmed, it should benefit from similar compactness-related capital cost savings. The GFR has the largest vessel (of pre-stressed cast iron type) among all four fast reactor concepts and employs 4× 50% large emergency cooling systems plus robust containment that needs to be designed for higher pressures than other contenders. On the other hand, it does not require IHXs, which are heavy and costly components. Nevertheless, it is expected the IHX savings will not overcome the increased cost of containment and large DHR loop components. Hence, the GFR will most likely have the largest capital cost, due to concrete and steel consumption, among the four concepts investigated.

4.2.4. Specific power

Specific power affects fuel cycle cost. While related to power density, specific power remains an independent variable whose value the designer strives to maximize to achieve acceptable fuel

cycle cost. Hejzlar et al. (2002) showed that the minimum specific power of 20 kW/kgHM should be achieved to keep fuel cycle cost within reasonable bounds. This was set as a minimum target for the development of FCR reactors in this project. All CR = 1 reactors achieved this target, albeit the GFR achieved only a 21 kW/kgHM value. As expected, the SFR has the largest specific power of 65 kW/kgHM, followed by the LFR with 45 kW/kgHM and the LSFR with 35 kW/kgHM. Cores with low specific power have a longer cycle length. Therefore, the GFR has a cycle length of 18 years and the SFR only 3.1 years. As discussed in Section 5, cycle length is limited by peak cladding fluence, which also determines achievable core-average discharge burnups. These are in the range of 70–80 MWd/kgHM for metallic fueled cores—relatively low values for fast reactors, signifying the importance of development of advanced cladding materials.

4.3. Safety

As for thermal reactors, fast reactors have to be designed to have excellent safety to protect the health of the public and the workers. The Generation IV program set the even more ambitious goal for nuclear energy systems to have a very low likelihood and degree of reactor core damage during any possible accident. To quantify the value of this likelihood requires a full probabilistic risk assessment (PRA), which is not possible at this point because the designs are only on a conceptual level. Therefore, the comparison of safety features of the four reactors in this study is focused on the results of deterministic analyses of key transients and identification of key issues or benefits that distinguish individual concepts. The discussion will focus specifically on the unprotected station blackout (SBO)[3], unprotected loss of flow (ULOF), and unprotected overpower (UTOP) accidents, since these events form an envelope of the initiators that lead to core heatup and can cause damage (except for the GFR where LOCA is the key bounding accident). The protected SBO will also be addressed since it can potentially lead to coolant freezing for some coolants. The whole spectrum of accidents, including hypothetical core disruptive accidents and seismic related events, will not be addressed.

In the spirit of the ambitious Generation IV goals, one of the objectives established before the start of this project was to achieve a level of safety that would exceed the already acceptable levels attained in currently operating reactors. While there are many possible approaches to achieve this goal, our selected approach was the achievement of the inherent, designed-in response of a reactor that would prevent release of radioactivity, as in the IFR. This requires a design that has: (1) a combination of reactivity feedbacks that inherently shut down the reactor without exceeding temperature limits on reactor structures in accidents without scram, and (2) a decay heat removal system based on natural phenomena that does not need external power. Such a combination of inherent and passive means is considered[4] to be highly reliable and potentially more economic than complex redundant active systems with reliable power supplies. It is also noted that including such unprotected accidents with extremely low probability goes far beyond the design basis and is not even considered in licensing the current generation of reactors.

4.3.1. Unprotected accidents

The plant response to unprotected accidents depends on two key features: the capability of inherent shutdown and the capability to remove decay heat passively. The following discussion will compare these two features in the four reactor concepts.

The IFR designers have proven by analysis that the sodium-cooled reactor with metal fuel can be designed to achieve the desirable self-controllability characteristics and transit to new asymptotic power levels under loss of heat sink (ULOHS), ULOF, and UTOP accidents without exceeding core material limits (Wade et al., 1997). Although the IFR and its successors, ALMR and PRISM, had relatively low power rating (up to 1000 MWt) due to limitations of RVACS passive decay heat removal, reactor physics analyses were applied to larger cores up to 3500 MWt. It was shown that it is possible to design large cores with reactivity feedbacks that achieve self-controllability, although smaller cores will achieve larger margins to cladding and fuel temperature limits (Wade and Hill, 1997). The SFR design in Table 2 is based on the 1000 MWt S-PRISM core, but the number of assemblies is increased to achieve a power of 2400 MWt for consistency with the other concepts. Table 6 in Section 5 shows that the A/B reactivity coefficient ratio is slightly above the self-controllability limit, indicating that the large core CR = 1 design may have difficulty achieving self-controllability. This is primarily due to larger positive CTC than for the small core. Since the large-core IFR design contains inner blankets, the CTC is reduced due to increased leakage of neutrons from the driver assemblies to the blanket assemblies upon coolant heatup. The CR = 1 core has no blankets and a low leakage core with flat power distribution, resulting in larger CTC. However, because the full design of the SFR core was beyond the scope of this project, no effort has been made in our SFR core calculations to reduce the CTC, as was the case for the lead- and salt-cooled reactors. Since the reduction of this reactivity coefficient needed to achieve self-controllability is small, it should be feasible to design a large SFR core with self-controllability features.

Reactor physics analyses (Shwageraus and Hejzlar, 2008, 2009) have shown that both the lead- and salt-cooled FCRs having CR = 1 can be designed for self-controllability. However, there is a significant difference between these two coolants. Lead coolant, due to its small thermal expansion coefficient, low absorption cross-section, low slowing down power and high scattering cross-section, exhibits only a small positive coolant temperature reactivity coefficient (CTC) (smaller than for SFR—see Section 5), which makes it possible to design a self-controllable CR = 1 core without the need for special features to mitigate the CTC. On the other hand, salt coolants, with their larger absorption cross-section and some moderating power, but most importantly their large coefficients of thermal expansion, exhibit a significant positive CTC that is difficult to overcome without introducing drastic measures into the core design or without introducing special, albeit passive devices. Ultimately, a salt core design with lithium expansion modules (LEMs), proposed originally by Kambe and Uotani (1998), which achieves zero or negative CTC and good self-controllability, was devised[5]. The difference among the SFR, LFR and LSFR is that the SFR and LFR can be designed to be self-controllable without such devices, while the LSFR requires them.

Gas coolants are neutron transparent and the CTC, or rather coolant void worth, is typically considered not to be an issue. However, there is a significant difference between liquid metal or

[3] The sodium-cooled IFR analyses are typically performed for unprotected loss of flow and unprotected loss of heat sink. Because the SBO is more challenging and because for a direct cycle GFR loss of flow is not independent of a loss of heat sink, unprotected SBO was selected for LFR and LSFR analyses.

[4] This does not necessarily apply to all reactors, as shown for the S-CO_2-cooled GFR design, where a combination of active and passive cooling was found preferable (Pope et al., 2009).

[5] LEMs are reservoirs of liquid lithium above the core connected to capillaries extending into the core. An increase in coolant outlet temperature causes lithium to thermally expand into the capillaries, reducing reactivity as neutrons are absorbed in the lithium. LEMs are able to passively introduce a strong negative reactivity feedback, making it much easier to achieve reactivity coefficients compatible with passive safety.

salt-cooled reactors and GFRs. GFRs operate at high pressure and can lose coolant rapidly for the postulated large pipe break, while the loss of coolant accident is not even analyzed for pool type liquid metal-cooled reactors having a guard vessel because of the extremely low probability of failure of both the reactor and guard vessels. Rapid coolant depressurization of the GFR core results in spectrum hardening and insertion of positive reactivity, which is very difficult to overcome through increased leakage—the principal means used to mitigate positive CTC in liquid metal reactors. It was also shown (Handwerk et al., 2006) that to make GFR self-controllable, coolant void worth needs to be negative—a significant difference from liquid metal-cooled cores, where other negative reactivity feedbacks can compensate for the slightly positive CTC. This is because in a GFR coolant depressurization in a large break LOCA can be very rapid and other reactivity coefficients may not have time to respond fast enough to achieve shutdown before material temperature limits are exceeded. A significant design effort has been made at MIT to achieve negative coolant void worth in the GFR design. This is accomplished in the S-CO_2 GFR by minimizing the coolant volume fraction through the use of TID assemblies, adding BeO diluent to UO_2 fuel and using S-CO_2 radial reflectors (Handwerk et al., 2006). Handwerk et al. (2006) also showed that the GFR can be designed as self-controllable at BOL, but not at EOL, due to less-negative coolant void worth. This has been confirmed by RELAP5 analyses for the unprotected LOCA by Pope et al. (2009).

The second feature of self-controllable design is the capability to remove sufficient stored energy passively immediately after shutdown as well as decay heat during the long term. This is especially challenging for reactors with a large power rating since the driving forces for natural phenomena are small and typically require large decay heat removal systems, negatively affecting capital cost.

The accompanying papers (Nikiforova et al., 2009; Petroski et al., 2009) show that the 2400 MWt lead- and salt-cooled FCR reactors with passive DHR systems can be designed to accommodate unprotected accidents, without the need for excessively large DHR systems. However, the enhanced RVACS alone was found to have insufficient performance and had to be supplemented with PSACS. Nonetheless, there were differences in performance between the lead- and salt-cooled concepts. While the LSFR can accommodate unprotected SBO without exceeding the peak cladding temperature limit for any number of operating PSACS trains with relatively small PSACS tanks, the lead-cooled reactor requires much larger tanks to keep peak cladding temperatures below the limit. This difference stems from the different CTCs of the individual reactors that lead to differences in primary system temperatures and reactor power in the long term restart, as explained next. During PSACS train operation (before PSACS tanks evaporate) the RVACS plus PSACS remove more heat than the decay heat generated in the core, which causes gradual reactor cooldown until primary temperatures reach a level when reactivity becomes zero and the reactor restarts to low power level (less than 10%). After reactor restart, its power and temperature stabilize at low levels that match the heat removal capacity of RVACS plus PSACS. During this period, the core temperatures remain constant until the water in the PSACS trains is evaporated. At this point, the primary system temperature rises, leading to reactor shutdown. Decay heat at this time is small enough to be removed by the RVACS. The LSFR with LEMs has net negative CTC, hence its power increase after restarts is smaller than that of the lead-cooled reactor, which has positive CTC. Therefore, the PSACS tanks for the lead-cooled reactor need to be significantly larger to maintain peak cladding temperature below the limit in the long term. Because larger tanks may not be economically attractive, one could also employ smaller tanks and scram the reactor manually or restore power. The operator has 24 h to initiate scram, which is ample time for such action. The LSFR does not need to scram and can maintain peak cladding temperature within limits for 72 h with smaller PSACS tanks, independent of the number of operating PSACS trains as long as 2 out of 4 trains are in operation.

The 1000 MWt SFR concept can rely fully on RVACS, and its self-controllability has been confirmed by S-PRISM analyses. The 2400 MWt SFR requires significant redesign of DHR systems. Section 3.2 discussed that it may be possible to use the same approach as for the LFR if a double-wall IHX is used to couple the SFR to the S-CO_2 PCS. Although not studied, it is expected that such a system would perform similarly as for the LFR after the SFR core design is optimized to reduce CTC.

The GFR DHR principle is very different from that of liquid metal-cooled reactors. The most promising concept is the use of DHR cooling loops that connect the low Δp core with elevated gas/water heat exchangers, all enclosed in a guard containment designed for a pressure of about 0.8 MPa. In case of a LOCA, the primary system and PCS depressurize into the containment, increasing containment pressure to an equilibrium of about 0.7 MPa. This pressure is sufficient to remove about 3% decay heat by natural circulation of CO_2 between the core and DHR HXs. However, detailed studies (Pope et al., 2006) have shown that there are many potential bypass paths (e.g., through double-ended break of coaxial pipes or through a PCS loop) that can lead to a significant reduction of core flow. Moreover, the startup of flow through a DHR loop in the correct direction is not reliable because leaky check valves can cause the reversal of temperature profiles in the DHR loop. Also, PRA studies of a helium-cooled GFR with a passive DHR system using uncertainty propagation have shown relatively high conditional damage frequency (Mackay et al., 2008; Patalano et al., 2008). For these reasons, it has been decided to abandon a fully passive DHR in the MIT GFR design. Battery or fuel cell powered, safety-grade, blowers are used and passive natural circulation is used as a backup. This is possible because blower power consumption is very low.

Overall, comparing the four concepts, it can be stated that all can be designed to accommodate the unprotected limiting accidents (easiest for LFR and most difficult for LSFR, which requires passive devices in the core), but it does not seem to be a preferable option in the GFR where the active or semi-passive approach will likely result in a more economic and more reliable plant. The benefit of using the S-CO_2 PCS is that it provides an additional heat removal option, since the decay heat can drive the turbine, which in turn drives the compressors to circulate CO_2 through the IHXs in a self-sustaining operational mode. This has been shown to be feasible and effective for the LFR and LSFR and could also be used in the SFR and GFR. However, this feature was not selected as the primary means for decay heat removal since making the power conversion system safety grade would significantly increase the cost.

4.3.2. Protected accidents

The probability of unprotected accidents is extremely low, thus these events are not even considered in the licensing process. Typically, one would expect that if the temperature constraints are met in a more challenging unprotected accident, they would also be met in the protected accident. However, this is not the case for liquid metal coolants, especially those with high melting points, since excessive heat removal can lead to primary system overcooling and coolant freezing. All three liquid cooled concepts are susceptible to this scenario, the SFR being less likely due to the large margin to melting point of sodium (254 °C), followed by the LFR (margin of 152 °C) and the LSFR (margin of 100 °C).

Analyses of the unprotected SBO for the LFR and LSFR confirmed that this is a significant issue, particularly for salt cores. When sizing the PSACS for the LFR, it was found that larger PSACS tanks are needed to accommodate the unprotected SBO. Because of the much higher probability of a protected SBO than an unprotected one, the plant needs to be designed to accommodate protected accidents. To avoid lead freezing in the protected SBO if all four PSACS

trains are operating, a small PSACS HX and large PSACS tank designs are needed. This combination was found to perform satisfactorily in both protected and unprotected accidents independently of the number of operating PSACS trains.

Design of the LSFR against freezing is particularly difficult, not only because of its smallest margin to freezing, but also because of its largest CTC coefficient. LEMs can be designed to compensate salt CTC in a limited temperature range, primarily to compensate for reactivity increase upon coolant heating. During core cooling below the nominal temperature, LEMs are out of the core and the large positive CTC yields strong power reduction during cooldown, speeding up reactor shutdown and thus increasing the core cooling rate. SBO analyses in the accompanying paper (Petroski et al., 2009) have shown that for the CR = 1 core and the PSACS tanks sized to accommodate the unprotected SBO (tank diameter/height = 6/12 m and 350 tube, 4 m long heat exchanger) the salt can freeze in about 20 h if the reactor is scrammed and 4 PSACS trains are operating. The best solution to this problem turned out to be the use of smaller PSACS tanks and heat exchangers. Petroski et al. (2009) shows that sizing the PSACS heat exchangers to transfer 40% less power (250 tubes, 2.4-long heat exchanger) than the original design and using 25% smaller PSACS tanks (D/H = 6/9 m) can accommodate both the unprotected SBO with peak cladding temperatures maintained below the 725 °C limit and the protected SBO without salt freezing.

Overall, protected accidents need to be given special attention in the LSFR and LFR due to their small margin to freezing, and to a lesser extent in the SFR. The GFR does not pose this challenge. The GFR's response to its most challenging event, the LOCA, will be significantly more benign than in the case of LOCA without scram.

5. Neutronic performance comparison

This section compares neutronic characteristics of the reactor concepts studied. The main design parameters of unity conversion ratio cores were described in Table 2. The comparison of different designs with respect to neutronic performance was focused on the following aspects:

- Potential of different designs to achieve high burnup and high power density as two major indicators of economic viability of the concepts.
- Potential of achieving near unity conversion ratio in a sustainable manner.
- Capability of self-control through passive design features in the most limiting accident scenarios.

The reactor designs discussed in this section have a significant number of common features, which allows consistent comparison among the concepts. All four designs have the same thermal power rating of 2400 MW and common design objectives of achieving a self-sustainable fuel cycle with respect to fissile feed requirements, while avoiding the use of fertile blankets, as well as maximizing power density and fuel burnup. Passive safety was also a common objective of all the designs. Neutronic analyses of the four designs were performed using the same methodology, assumptions and simulation tools: MCODE, BGCore, MCNP described in Todreas et al. (2008). In addition, the calculations were performed using the same JEFF-3.1 cross-section data libraries, unless stated differently.

Metallic U–TRU–Zr fuel was used in all reactors except for the GFR, where high temperatures and compatibility requirements with CO_2 coolant necessitate use of oxide fuel. The initial TRU composition was also identical in all the reactor concepts and corresponded to that of a typical spent LWR fuel with 50 MWd/kg burnup after 10 years of cooling. Single batch fuel management strategy was used in all the compared designs. The approach to power distribution management by tailoring a diluent content in the radial fuel zones while keeping the TRU to uranium ratio constant was proven to be very effective. The maximum radial power peaking factors do not exceed 1.3 in all core designs, without significant change with fuel burnup.

Table 3
Comparison of core average neutron flux.

	GFR	Lead	Salt	Na
Flux, average over the cycle (n/(cm^2 s))	1.05×10^{15}	2.82×10^{15}	2.73×10^{15}	4.89×10^{15}
Fraction of fast neutrons >0.1 MeV	0.49	0.69	0.69	0.70
Cycle length, days	6000	1800	1800	1150

In all of the considered cases, the fuel burnup was constrained by the peak cladding fluence. Therefore, all the liquid-cooled reactor cores have approximately the same discharge burnup (Table 2). The limit of 4×10^{23} (neutrons above 0.1 MeV)/cm^2 roughly translates for liquid metal and salt-cooled reactors into 70–80 MWd/kg of burnup. The small differences in discharge burnup can be attributed to slightly different neutron spectra and calculation uncertainty. GFR fuel has a notably higher burnup of 140 MWd/kg. This is partially due to a softer spectrum (only 49% of GFR neutrons are above 0.1 MeV versus 69% for the lead-cooled reactor), but most importantly due to significantly lower core-average neutron flux. The much smaller neutron flux of the GFR core is the consequence of significantly higher heavy metal, and in particular TRU loading, and thus higher number density of fissile isotopes. This can be also inferred from the significantly smaller GFR specific power. The neutron flux comparison among the concepts is given in Table 3. In addition, the GFR uses ODS steel as cladding, which is expected to have a higher fluence limit than HT-9 steel. GFR cladding has an accumulated peak fluence of 4.7×10^{23} n/cm^2 ($E > 0.1$ MeV). This is within the limit of 5×10^{23} n/cm^2 ($E > 0.1$ MeV) used by Japanese designers for JSFR with ODS cladding (Mizuno et al., 2005). In addition, the unique TID fuel assembly design allows controlled venting of the fission gases and, thus, more flexibility in managing the mechanical stresses within the assembly.

Significant differences between the cores affecting neutronics stem from differences in achievable power densities. The power density is related to a combination of heat transfer properties of the respective coolants, as discussed in Section 6. Sodium coolant, with its exceptionally good heat transfer properties, has a clear advantage, which results in two to three times higher power density than those of the other concepts. Therefore sodium reactors have much smaller cores, and thus a smaller heavy metal loading and larger neutron flux, as shown by comparing Tables 3 and 4. The SFR flux is about twice as large as that of the lead-cooled reactor.

In the lead- and salt-cooled reactors, additional considerations play an important role in setting the coolant volume fraction. For the lead coolant, there is a limit on coolant velocity, required to prevent corrosion of the core structural components. As a result, a relatively

Table 4
Heavy metal inventory comparison of CR = 1 core designs.

	Lead	Salt	S-CO_2	Na
Core initial HM loading (kg)	56,472	67,847	115,711	35,444
Pu	8,131	9,202	17,203	4,662
MA	1,255	1,421	1,905	720
NU	47,086	57,224	96,604	30,062
Core HM inventory at discharge (kg)	51,878	61,719	99,261	32,616
Pu	8,268	9,533	18,774	4,856
MA	953	1,058	1,278	536
NU	42,657	51,128	79,209	27,224
Fissile inventory ratio, discharged/loaded	0.98	1.00	1.05	1.00

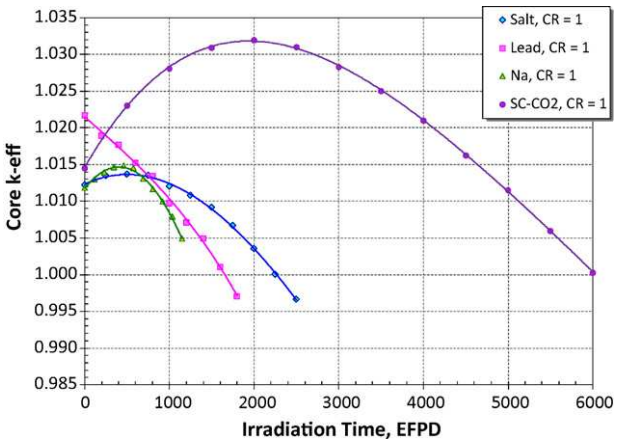

Fig. 8. CR = 1 core multiplication factors versus irradiation time.

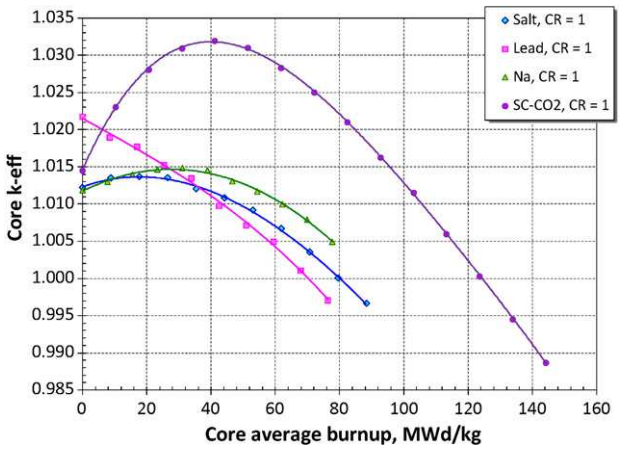

Fig. 9. CR = 1 core multiplication factors versus core average burnup.

open fuel lattice has to be used, which limits the power density to values comparable to conventional LWRs. Fortunately, an open lattice of the lead core is feasible without significantly increasing the coolant temperature coefficient. This is because of the relatively low lead absorption cross-section and the high scattering cross-section that increases leakage upon coolant voiding.

For the salt, the large positive CTC necessitates a small coolant volume fraction in order to minimize the reactivity insertion upon coolant heatup. However, the high viscosity for most of the molten salts limits the achievable power density for a given pumping power constraint. Using some innovative design strategies to reduce the CTC (as discussed in accompanying paper by Shwageraus and Hejzlar, 2009) or reliance on redundant special shutdown mechanisms, allows one to somewhat relax the constraint on the coolant volume fraction and achieve a power density of 130 W/cm^3. This is notably higher than in the lead-cooled core, but still far from the sodium-cooled core power density by over a factor of two. Moreover, it needs to be noted that without these passive reactivity devices, the power density of salt-cooled reactors would be limited to about 70 kW/l, even if the core pressure drop is ~2 times higher than the typical values for sodium fast reactors.

Variation in achievable power density for fixed total power leads to large differences in volume of the studied cores (Table 2). Generally, all the designs have a relatively small core height and height-to-diameter ratio to minimize the core pressure losses, and take advantage of large neutron leakage in order to mitigate the positive CTC common in all fast reactors. While power density has an impact on economic viability of each reactor design, specific power is an important indicator of fuel cycle cost competitiveness. In this respect, the lead-cooled core has certain advantages over the salt because of the looser fuel lattice of the former. In spite of the very tight lattice achievable in the sodium-cooled core, very high power density also leads to the highest specific power among all the designs (Table 2).

Reactivity of the studied cores as a function of time and core average burnup are plotted in Figs. 8 and 9, respectively. The GFR core has the longest fuel cycle of about 18 years and the highest discharge burnup because of the combination of the following factors: high heavy metal loading (and thus low neutron flux and cladding fluence), large dimensions, and relatively low specific power. The sodium-cooled reactor, on the other hand, reaches its fluence-limited-burnup relatively fast due to the high specific power. The cycle length of the 1-batch lead- and salt-cooled reactors is on the order of 5 years, which is roughly comparable to a typical LWR fuel residence time in a 3-batch core.

Table 4 summarizes the balances of materials in the compared designs. The last line of the table gives a fissile inventory ratio (FIR) defined as the discharged mass of TRU divided by the TRU initially loaded. All the designs can achieve a FIR of about unity. In all cases, the relative fraction of Pu increases, while the fraction of MA decreases. It was shown that the recycled first generation TRU is sufficient to sustain the next fuel cycle for at least the same length with natural uranium makeup only.

Similarities in the neutronic performance of the compared cores can be attributed to the fact that all cores have generally similar neutron spectra despite the differences in the coolants and lattice geometries. Neutron spectra for all the reactor concepts are presented in Fig. 10. Significant differences can be observed only in GFR core regions with large BeO content. Otherwise, the neutron spectra are very similar. This observation is supported by the comparison of one-group cross-sections calculated for the most important actinides in all reactor types (Table 5). Only minor variations in the cross-sections can be observed, with no clear advantage of one coolant type over the other. As a result of such minor differences, the goal of achieving near unity conversion ratio with about the same initial enrichment can be achieved by all the considered reactors. This may be surprising since one could expect that the sodium and salt coolants with their larger moderating power (see Table 1) would yield softer spectra. However, optimization of each core design for the achievement of CR = 1 and of satisfactory reactivity coefficient ratios results in various coolant to fuel volume ratios among various core designs and addition of moderating diluent in case of GFR, so that similar spectra are achieved.

A key figure of merit for comparison of different core designs is their potential for self-controllability in the most restricting accident scenarios, by passive means. The quasi-static safety analysis

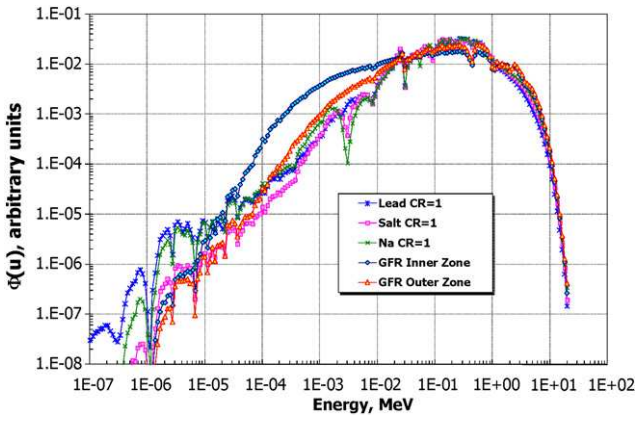

Fig. 10. Comparison of neutron spectra in CR = 1 cores.

Table 5
One-group cross-section comparison for different reactor types (barns).

Nuclide (ZZAAA)	GFR (CR = 1)				SFR (CR = 1)			
	$\sigma(n,\gamma)$		$\sigma(n,\gamma)$		$\sigma(n,\gamma)$		$\sigma(n,\gamma)$	
	Outer	Inner	Outer	Inner	Outer	Inner	Outer	Inner
92235	0.51	0.89	1.83	2.59	0.43	0.47	1.65	1.73
92238	0.25	0.38	0.05	0.05	0.22	0.24	0.04	0.03
94238	0.50	0.96	1.26	1.49	0.41	0.46	1.16	1.15
94239	0.45	0.93	1.75	2.19	0.34	0.39	1.68	1.70
94240	0.45	0.81	0.42	0.38	0.38	0.41	0.38	0.35
94241	0.45	0.75	2.44	3.40	0.38	0.42	2.21	2.31
94242	0.45	0.77	0.30	0.27	0.36	0.40	0.27	0.24

Nuclide (ZZAAA)	LFR (CR = 1)				LFR (CR = 0)			
	$\sigma(n,\gamma)$		$\sigma(n,\gamma)$		$\sigma(n,\gamma)$		$\sigma(n,\gamma)$	
	Outer	Inner	Outer	Inner	Fresh	Twice	Fresh	Twice
92235	0.42	0.43	1.64	1.65	0.50	0.50	1.80	1.79
92238	0.22	0.23	0.03	0.02	0.32	0.29	0.03	0.02
94238	0.41	0.41	1.15	1.13	0.49	0.48	1.22	1.18
94239	0.34	0.35	1.66	1.65	0.44	0.44	1.75	1.71
94240	0.38	0.38	0.36	0.34	0.44	0.43	0.38	0.34
94241	0.38	0.39	2.20	2.21	0.45	0.44	2.41	2.38
94242	0.36	0.37	0.25	0.23	0.44	0.43	0.27	0.24

Nuclide (ZZAAA)	LSFR (CR = 1)				LSFR (CR = 0)			
	$\sigma(n,\gamma)$		$\sigma(n,\gamma)$		$\sigma(n,\gamma)$		$\sigma(n,\gamma)$	
	Outer	Inner	Outer	Inner	Fresh	Twice	Fresh	Twice
92235	0.41	0.43	1.62	1.66	0.51	0.54	1.81	1.87
92238	0.22	0.23	0.03	0.03	0.31	0.32	0.04	0.03
94238	0.39	0.42	1.15	1.14	0.49	0.52	1.25	1.22
94239	0.33	0.36	1.65	1.65	0.45	0.49	1.75	1.76
94240	0.36	0.38	0.37	0.35	0.44	0.47	0.40	0.36
94241	0.37	0.39	2.17	2.23	0.45	0.47	2.42	2.49
94242	0.35	0.37	0.26	0.25	0.44	0.47	0.29	0.25

approach, introduced by Wade and Chang (1988) for the IFR and described for lead- and salt-cooled reactors in Todreas et al. (2008), was adopted in order to assess this potential. The results of the reactivity coefficients and self-controllability criteria calculations are summarized in Table 6. For the liquid metal and salt-cooled cores, the Doppler reactivity coefficient is practically the same because it is primarily determined by the fuel composition and spectrum, which is similar in all cases. The GFR oxide fuel core has a more negative Doppler coefficient due to its softer spectrum in the inner core with its BeO diluent. Also, the actual reactivity feedback due to the Doppler effect differs between metal-fueled cores and the oxide-fueled GFR because of significantly larger fuel temperature change per unit of power change as a result of the smaller UO_2 thermal conductivity.

The fuel and core radial thermal expansion coefficients depend on a combination of fuel lattice and core geometry but still appear to be very similar for all the designs, except for the GFR, which with its low-coolant-fraction tube-in-duct (TID) assembly exhibits an appreciably smaller core radial expansion coefficient. The common knowledge is that the CTC is larger for coolants with higher mod-

Table 6
Summary of reactivity feedback parameters (at BOL).

	Units	LFR	±σ	LSFR	±σ	SFR	±σ	GFR	±σ
β		0.0036	0.0001	0.0039	0.0001	0.0038	0.0001	0.0045	0.0002
α_{DC}	¢/K	−0.111	0.030	−0.092	0.030	−0.130	0.030	−0.355	0.017
α_e	¢/K	−0.117	0.026	−0.050	0.022	−0.091	0.018	−0.043	0.009
α_{Co}	¢/K	+0.131	0.052	−0.040	0.044	+0.156	0.041	−108¢[a]	7
α_{RD}	¢/K	~0	N/A	~0	N/A	~0	N/A	~0	N/A
α_R	¢/K	−0.135	0.013	−0.159	0.022	−0.145	0.018	−0.049	0.003
A	¢	−22.92	3.99	−15.66	3.32	−44.19	7.03	−238	9
B	¢	−17.43	2.43	−22.43	2.61	−26.67	4.25	−38	2
C	¢/K	−0.23	0.05	−0.38	0.06	−0.21	0.06	−0.45	0.03
A/B		1.31	0.29	0.70	0.06	1.66	0.37	See[b]	
$C\Delta T_c/B$		1.27	0.31	1.40	0.11	1.18	0.36	See[b]	
$\Delta\rho_{TOP}/B$		0.33	0.05	0.24	0.01	1.05	0.17	See[b]	
A/B limits		$x < 1.06$ (1.59[c])		$x < 1.15$ (1.73)		$x < 0.99$ (1.49)		See[b]	
$C\Delta T_c/B$ limits		$1 < x < 1.99$ (2.39)		$1 < x < 2.36$ (2.94)		$1 < x < 1.90$ (2.25)		See[b]	
$\Delta\rho_{TOP}/B$ limits		$x < 1.06$ (1.59)		$x < 1.15$ (1.73)		$x < 0.99$ (1.49)		See[b]	

[a] Coolant temperature coefficient for GFR is negligible. Value given is coolant void worth, i.e., reactivity change when *all* coolant is voided after LOCA.
[b] The direct cycle GFR quasi-static method (DCGQSM) differs from the traditional method used for liquid metal-cooled reactors, because a loss of flow cannot occur without a degradation of heat sink in a direct cycle system and because coolant voiding in LOCA affects a GFR core differently than the liquid metal-cooled cores. Therefore, the reactivity coefficient ratios and their limits are different, as described in Handwerk et al. (2007).
[c] Values in parentheses do not include margin for power peaking.

erating power and larger absorption cross-section. However, for these effects to come into play for liquid coolants, there is another underlying coolant thermophysical property that determines the CTC—the thermal expansion coefficient. Lead has the smallest CTC due to its smallest thermal expansion coefficient and low moderating power, while the salt-cooled core exhibits the largest CTC because of its highest thermal expansion coefficient, high moderating power and largest absorption cross-section. Negative CTC in the salt core reported in Table 6 was achieved due to the use of lithium thermal expansion modules (LEMs), described in the accompanying paper by Shwageraus and Hejzlar (2009). Without the LEMs, the salt-cooled core would have a positive CTC of about 0.80 ¢/K, which is larger than the CTC of the lead or sodium-cooled cores by over a factor of five. A core with such a large positive CTC cannot satisfy self-controllability criteria. The GFR has a negligible coolant temperature coefficient. Rather, it is coolant void worth, or reactivity change upon loss of coolant, which is of primary importance in safety analyses, and it is thus reported in Table 6. The SCO_2-cooled core design exhibits negative coolant void worth due to use of low-coolant fraction TID assemblies with addition of BeO diluent, and the use of S-CO_2 reflectors that assure increased leakage upon loss of coolant. Negative coolant void worth is a unique feature of this GFR design, and as shown in Handwerk et al. (2007), a necessary condition to satisfy self-controllability requirements.

Overall, it can be stated that the cores for all coolants can be designed to satisfy self-controllability requirements. However, different levels of effort and measures for each core are necessary to achieve this goal. Lead coolant is the most attractive coolant for satisfying the self-controllability criteria, due to its small absorption, small moderating power and high scattering cross-sections. The sodium-cooled core is more challenging due to its larger CTC. Table 6 shows that the limit on the A/B ratio for the sodium-cooled core is not satisfied, hence more optimization would be needed to meet this limit for this particular core. However, prior work (Wade and Chang, 1988) shows that this is possible without the need to introduce special reactivity devices. The salt-cooled cores are extremely difficult to design for self-controllability. The proposed salt-cooled core satisfies all the criteria exclusively due to the use of LEMs. This difficulty also holds for GFRs, where it is necessary to achieve negative coolant void worth to achieve this goal. This is because coolant depressurization in large LOCA can occur rapidly, before other reactivity feedbacks can respond. Although it is a truly challenging task to design a core with negative coolant void worth, it is not impossible, as shown in Handwerk et al. (2007).

6. Thermal hydraulic performance comparison

Thermal hydraulic comparison is based on several figures of merit that are important for operating characteristics of the reactor cores. Since sodium is known to have the best thermal hydraulic characteristics among fast reactor coolants, the compared parameters are normalized to those of sodium. The summary of the normalized compared quantities is provided in Tables 7 and 8. Table 7 lists the key figures of merit while Table 8 summarizes the complimentary metrics.

6.1. Figure of merit #1—core power density

Core power density is a figure of merit for core and vessel size. Core size is directly related to the capital cost of the reactor. Therefore, if the core size is reduced for the same power generated, fewer fuel assemblies are used, reducing the cost of the core. It also allows reduction of the vessel size, although this may not be the case for passive decay heat removal systems which use the vessel as a heat transfer surface and thus favor a large vessel size. Even for the reactors having passive DHR, high power density cores provide more space for the placement of heat exchangers and pumps and for refueling storage space, thus simplifying the system and reducing the cost. Therefore, it can be stated that high power density leads to

Table 7
Key figures of merit[a].

	Metric #	GFR	SFR	LFR	LSFR
Core power density (kW/l)	1	85.4	290	112	104
Power density ratio					
Norm to Na		0.294	1.000	0.386	0.359
Norm to Pb		0.763	2.589	1.000	0.929
ρc_p (J/(cm^3 K))	2	0.18	1.07	1.55	1.92
Stored heat ratio					
Norm to Na		0.168	1.000	1.449	1.794
Norm to Pb		0.116	0.690	1.000	1.239
Pumping power (MW)	3	34.3	3.82	7.41	3.45
Pumping power ratio					
Norm to Na		8.997	1.000	1.943	0.903
Norm to Pb		4.630	0.515	1.000	0.465
Heat transfer coefficient	4	6529.791	180607.467	28139.388	5808.923
Norm to Na		0.036	1.000	0.156	0.032
Norm to Pb		0.232	6.418	1.000	0.206
FOM[b]-forced convection, turbulent	5	766.111	30.195	122.252	19.125
Norm to Na		25.372	1.000	4.049	0.633
Norm to Pb		6.267	0.247	1.000	0.156
FOM[b]-natural convection, turbulent	5	70.078	40.425	43.571	27.892
Norm to Na		1.734	1.000	1.078	0.690
Norm to Pb		1.608	0.928	1.000	0.640
FOM[b]-natural convection, laminar[a]	5	61.289	64.371	68.448	98.326
Norm to Na		0.952	1.000	1.063	1.527
Norm to Pb		0.895	0.940	1.000	1.436

[a] All properties are for 450 °C; properties of CO_2 are for 20 MPa pressure; laminar flow is only for LSFR transients.
[b] Figure of merit (FOM)—for these factors a smaller value is preferable.

Table 8
Complimentary metrics of thermal hydraulic parameters[a].

	GFR	SFR	LFR	LSFR
Mass flow rate through the core (kg/s)	11,708	13,580	173,600	29,000
Mass flow rate				
Norm to Na	0.862	1.000	12.784	2.135
Norm to Pb	0.067	0.078	1.000	0.167
Pressure drop through active core (Pa)	421,500	236,584	450,000	227,000
Pressure drop ratio				
Norm to Na	1.782	1.000	1.902	0.959
Norm to Pb	0.937	0.526	1.000	0.504
Reynolds number	613979.2	74916.4	83608.3	6003.4
Norm to Na	8.196	1.000	1.116	0.080
Norm to Pb	7.344	0.896	1.000	0.072
Prandtl number	0.7581	0.0050	0.0192	8.9330
Norm to Na	151.620	1.000	3.840	1786.600
Norm to Pb	39.484	0.260	1.000	465.260
Nusselt number	816.224	7.379	14.328	49.003
Norm to Na	110.621	1.000	1.942	6.641
Norm to Pb	56.968	0.515	1.000	3.420
Coolant velocity, average (m/s)	21.112	8.533	2.034	3.315
Velocity ratio				
Norm to Na	2.474	1.000	0.238	0.388
Norm to Pb	10.379	4.195	1.000	1.630

[a] All properties are for 450 °C; properties of CO_2 are for 20 MPa pressure; laminar flow is only for LSFR transients.

lower capital cost. Because of the superior thermal hydraulic characteristics of sodium coolant, its power density is about three times the power densities of the other reactors evaluated in this project. As expected, the S-CO_2-cooled reactor exhibits the lowest power density.

It is interesting to note the significantly smaller power density of the lead-cooled core in comparison to sodium. This is to a large extent the consequence of the velocity constraint imposed to prevent erosion of oxide film. To keep the coolant velocity within the 3 m/s constraint, the lead-cooled cores must have a higher coolant volume fraction. Increasing core coolant volume fraction by opening the core lattice is possible neutronically, as discussed under the neutronic section, but negatively impacts the core power density. Smaller power density requires a larger lead-cooled active core, but due to the high density of lead and its excellent scattering cross-section, radial reflectors and shields to attenuate gamma-rays and energetic neutrons are not required for lead-cooled reactors, which somewhat compensates for the core size difference.

6.2. Figure of merit #2—heat storage capacity

The amount of heat that can be stored in the primary coolant is important during transient conditions. Cores having coolants with a greater capacity to absorb decay heat exhibit milder transient response and lower peak cladding and fuel temperatures. All liquid cooled reactors have a large capacity to store decay heat. Therefore, long times (on the order of hours) to reach peak cladding temperatures are characteristic for these coolants during accidents with loss of heat sink. This is different for the GFR. Although the GFR has a very large coolant volume because of the direct coupling to the PCS, and the gas is kept at a very high pressure to maintain coolant heat capacity as high as possible, the heat storage capability is still well below that of liquid metals or salts. Moreover, gas coolant escapes rapidly during large LOCA events, drastically reducing heat storage capacity. In this metric, salt coolant shows the best performance, mainly because of its large specific heat, followed by lead, which has large density.

6.3. Figure of merit #3—pumping power

The pumping power ratio through the core is an important figure of merit because it affects power consumption and thus net plant efficiency. The goal is to minimize the pumping power to increase the "useful" power production:

$$\frac{\text{Pump power}_1}{\text{Pump power}_2} = \frac{\Delta P_1}{\Delta P_2} \cdot \frac{\dot{m}_1 \rho_2}{\dot{m}_2 \rho_1}. \quad (1)$$

Pumping power depends on mass flow rate and core pressure drop. Mass flow rates for fixed core power depend on core temperature rise and the specific heat capacity of the coolant. Therefore, the ratio of flow rates and pressure drops needs to be established. The flow rate ratio is:

$$\frac{\dot{m}_1}{\dot{m}_2} = \frac{(\dot{Q}/(T_{out} - T_{in})c_p)_1}{(\dot{Q}/(T_{out} - T_{in})c_p)_2} = \frac{((T_{out} - T_{in})c_p)_2}{((T_{out} - T_{in})c_p)_1}. \quad (2)$$

Since all reactor concepts in this comparison employ the S-CO_2 PCS, which optimizes at a temperature rise across a heat source close to 150 °C, all reactor concepts have a similar core temperature rise. Therefore, the mass flow ratios are roughly inversely proportional to the specific heats. Because lead has almost 10 times lower specific heat than sodium, its mass flow rate is about 10 times higher.

The second parameter, the pressure drop ratio across the reactor core, is an important parameter affecting not only pumping power but also liftoff forces acting on fuel assemblies. Moreover, low pressure drop is important for systems relying on passive decay heat removal. A small pressure drop results in increased natural circulation of the coolant. Generally, the sodium-cooled reactor core pressure drop is small (factor of 3–5 smaller) compared to that of lead or salt. However, because of the small hydraulic diameter (tight core) and high coolant velocity, the pressure drop through the active sodium core is comparable to that of the lead-cooled core (~only factor of 2 smaller than lead). The larger pressure drop of the lead-cooled core comes from the much higher density of lead versus sodium and the use of grid spacers in the lead square lattice, versus wire wraps in hexagonal lattices. These two aspects more than

counterbalance the effect of lower lead velocity. It may be surprising that the pressure drop of the liquid salt reactor is comparable to that of sodium, and smaller than that of the LFR, in spite of the high viscosity of liquid salt. This is due to the much smaller velocity of the salt coolant versus sodium and its low density as compared to lead.

Given the mass flow rate and pressure drops of the cores under comparison, the lead-cooled reactor exhibits about two times larger pumping power than the sodium- and salt-cooled designs. This is primarily because of the larger pressure drop of the lead-cooled core, since the flow rate over density ratios are about the same for both coolants. As expected, the GFR has the largest core pumping power because of small coolant density. However, since the GFR is a direct cycle plant and compressor pumping power is part of PCS efficiency calculations, it does not lead to additional plant efficiency reduction in a transparent manner. For indirect cycle plants, this pumping power would have a significant negative impact on plant efficiency, since it would have to be included separately through main gas coolant circulators.

6.4. Figure of merit #4—heat transfer coefficient

Heat transfer coefficient is a key parameter affecting the film temperature and thus cladding peak temperature. It is directly proportional to Nusselt number and coolant conductivity and indirectly proportional to hydraulic diameter:

$$h = \frac{Nuk}{D_h}, \tag{3}$$

where Nusselt number is typically proportional to the *Re* and *Pr* numbers. For gases and liquid salt (Gnielinski, 1976):

$$Nu = 0.0214(Re^{0.8} - 100)Pr^{0.4}. \tag{4}$$

For lead and sodium, the correlation developed by Westinghouse (Todreas and Kazimi, 1993) for metallic fluids flowing through rod bundles was used:

$$Nu = 4.0 + 0.33\left(\frac{P}{D}\right)^{3.8}\left(\frac{Re\,Pr}{100}\right)^{0.86} + 0.16\left(\frac{P}{D}\right)^{5.0}. \tag{5}$$

The Reynolds number:

$$Re = \frac{\rho V D_h}{\mu}, \tag{6}$$

measures the ratio of inertia force to viscous force and is proportional to density, velocity and hydraulic diameter, and indirectly proportional to the dynamic viscosity of the fluid. As shown in Table 8, the largest *Re* number is for the GFR. This is a result of the high velocity and small kinematic viscosity of CO_2. On the other side of the range is the LSFR, which has a much smaller *Re* number than either the sodium-cooled or the lead-cooled reactors. The very low *Re* number of liquid salts is primarily the consequence of high salt viscosity.

The Prandtl number, which is the ratio of momentum diffusivity to thermal diffusivity, differs among each coolant as indicated in Table 8. The largest value is for the salt-cooled reactor due to high salt viscosity and the smallest is for sodium coolant, primarily due to its high conductivity. For lead, and sodium, thermal diffusivity is dominant; hence heat conduction is more effective than convection. The thickness of the velocity boundary layer of salt and gas is bigger than the thermal boundary layer, resulting in effective convection.

Using Eqs. (4) and (5) yields Nusselt numbers shown in Table 8. One can observe that lead and sodium coolants have relatively low *Nu* numbers, primarily due to their high thermal conductivity. On the other hand, CO_2 has the largest *Nu* number due to its small conductivity and large Reynolds number.

Finally, using Eq. (3), one can obtain heat transfer coefficients, *h*, listed in Table 7. The heat transfer coefficient of metallic coolants (especially sodium) is significantly higher than for the other fluids. Even though the *Nu* number of sodium is smaller than that of lead, its heat transfer coefficient is over 6 times larger although the thermal conductivity of sodium is only four times that of lead. The difference comes from much smaller hydraulic diameter of the sodium lattice, since neutronic properties require a tight lattice for the sodium core, while the velocity constraint for lead coolant demands a loose lattice. Gas and salt are the opposite of the metals, with very low heat transfer coefficients as a result of their low conductivity, in spite of their large *Nu* numbers. The small heat transfer coefficient of the LSFR, even slightly smaller than that of the S-CO_2-cooled GFR, is a surprising result. It is a consequence of the very high viscosity of salt coolants, which leads to small *Re* numbers.

6.5. Figure of merit #5—minimum pumping power for fixed coolant temperature rise

The other generalized heat transfer metrics used were originally developed by Bonilla (1958) and later employed in simplified form by Williams et al. (2006). The figures of merit (FOM) are based on minimal pumping power for a given coolant temperature rise as the objective function for forced convection

$$\mathrm{FOM(forced\ convection,\ turbulent)} = \frac{\mu^{0.2}}{\rho^2 c_p^{2.8}} \tag{8}$$

Salt is the best for the given temperature, and gas shows the highest requirements for the pumping power. The forced convection FOM agrees well with the pumping power metric described earlier, i.e., the smallest values for salt followed by sodium, lead and CO_2 coolants.

For natural convection cooling the following FOMs originally derived by Bonilla can be used:

$$\mathrm{FOM(natural\ convection,\ turbulent)} = \left[\frac{\mu^{0.2}}{\beta\rho^2 c_p^{1.8}}\right]^{0.357} \tag{9}$$

$$\mathrm{FOM(natural\ convection,\ laminar)} = \left[\frac{\mu}{\beta\rho^2 c_p}\right]^{0.5} \tag{10}$$

The above two FOMs measure the efficiency of a coolant to dissipate heat with low coolant temperature rise and are applicable to any coolant. The response of the reactor during accident conditions is difficult to estimate without detailed simulation. It is important to note that the above FOMs are figures of merit of potential performance of coolants without incorporating the impact of system geometry. However, the presented metrics can provide the first insight into the potential of various coolants to effectively dissipate heat. The smaller number corresponds to the better performer.

Turbulent natural convection results rate the coolants similarly as for forced convection, with salt being the best performer (primarily due to its large ρc_p) followed by sodium, lead, and gas as the worst performing coolants. However, the low Reynolds number of salt coolant suggests that turbulent conditions under accidents involving loss of pumping power (natural circulation) are unlikely. Moreover, laminar conditions are unlikely for sodium, lead, and gas coolants because of their thermal hydraulic characteristics discussed earlier. Therefore, the natural circulation conditions must be compared for the laminar regime, for the salt reactor, and for the turbulent regime for the other reactors. Based on those conditions, sodium becomes the best coolant for the natural circulation condition, with lead coolant following it very closely.

6.6. Other parameters of interest

Coolant velocities are also important as they affect both pressure drops and heat transfer as well as mechanical aspects of the core design to prevent vibrations and structure wear. Table 8 shows the coolant velocity ratio:

$$\frac{v_1}{v_2} = \frac{(A_c(T_{out} - T_{in})\rho c_p)_2}{(A_c(T_{out} - T_{in})\rho c_p)_1}. \quad (7)$$

It depends on coolant density and coolant volume fraction in the core. In spite of having the largest mass flow rate, the lead-cooled core has the smallest velocity. The mass flow rate is high because of the large density of lead and an open core lattice, but the velocity is kept low because of the limit imposed by the corrosion constraint. The coolant velocity in lead reactors is limited to 3 m/s because of corrosion issues, in contrast to sodium reactors where coolant velocities can reach 8–10 m/s. Low coolant velocity in a lead-cooled core affects the heat removal capabilities and consequently the cladding temperatures and reactor operating temperatures. The constraint on low lead coolant velocity limits the heat removal capacity of the lead reactor and requires an open lattice. On the other side of the spectrum is the S-CO_2-cooled GFR, where the small density and coolant volume fraction of CO_2 require a large coolant velocity to attain CR = 1 with the lower heavy metal density UO_2 fuel.

7. Summary and conclusions

Four fast reactor concepts using lead, liquid salt (NaCl–KCl–$MgCl_2$ (30–20–50)), sodium, and S-CO_2 coolants were compared. Since the conceptual designs of all these reactors were developed with emphasis on Generation IV goals, have identical power rating of 2400 MWt and employ the same S-CO_2 power conversion system, the comparison provides a unique opportunity to determine the impact of different coolants on reactor design and its key operating and safety characteristics.

Although all reactors can be designed with flexible conversion ratio, the comparison focused on unity conversion ratio reactors because they address both the efficient utilization of uranium resources as well as reduce the long-term stewardship burden by depleting legacy TRU from spent LWR fuel. In fact, in a nuclear energy growth scenario, the CR = 1 reactors can deplete legacy TRU by the same date as CR = 0 units due to the large heavy metal loading of fast reactor first cores. Because a large number of either CR = 1 or CR = 0 reactors (although 7 times more CR = 1 versus CR = 0 fast reactors) is needed to accomplish TRU management, it is critical that their cost becomes competitive with that of LWRs in order to be preferred by utilities. Hence, attractive fast reactor economics needs to be a major effort in the design of future systems.

Regarding economics, since economy of scale and power conversion system compactness are the same by virtue of the consistent 2400 MWt rating and use of the S-CO_2 power conversion system, the achievable plant thermal efficiency, core power density and core specific powers were compared. Operating coolant temperatures and fuel linear power and compactness become the dominant factors. The potential to achieve the highest efficiency among the four reactor concepts can be ranked from highest to lowest as follows: (1) GFR, (2) LFR and LSFR, and (3) SFR. On the other hand, the GFR is the least compact system and requires robust containment. Both the lead and salt designs achieve about 30% higher power density than the gas-cooled reactor, but have a power density 3 times smaller than that of the sodium-cooled reactor. However, for the sodium concept to benefit from capital cost savings from this smaller potential core size, the decay heat removal approach also needs to keep the reactor vessel size suitably bounded. Fuel cycle costs are favored for the sodium reactor by virtue of its high specific power 65 kW/kgHM compared to the lead, salt and gas reactor values of 45, 35, and 21 kW/kgHM, respectively.

In terms of safety, all concepts can be designed to accommodate the unprotected limiting accidents. However, it does not seem to be a preferable option in the GFR, where the active or semi-passive approach will likely result in a more economic and more reliable plant. Lead coolant with its superior neutronic characteristics and the smallest coolant temperature reactivity coefficient is easiest to design for self-controllability, while the LSFR requires special reactivity devices, such as liquid expansion modules to overcome its large positive CTC. The GFR required a special core design using BeO diluent in the core and a S-CO_2 reflector to achieve negative coolant void worth—one of the conditions necessary for inherent shutdown following large LOCA. Protected accidents need to be given special attention in the LSFR and LFR due to their small margin to freezing, and to a lesser extent in the SFR. The GFR does not pose this challenge. Finally, the well known vulnerability of sodium to its chemical reaction with water is to be noted should the Rankine power conversion cycle be utilized. As well of note is the opacity of both sodium and lead, as it would affect under surface in-vessel fuel handling operations.

Acknowledgments

The support provided by the U.S. DOE Nuclear Energy Research Initiative (NERI) for this project on flexible conversion ratio fast reactors is gratefully acknowledged. The comparison presented in this paper also benefits from prior MIT work on the development of the supercritical CO_2-cooled direct cycle gas-cooled fast reactor under another U.S. DOE funded NERI project and GEN IV funding via Sandia National Laboratory on Qualification of the Supercritical CO_2 Power Conversion Cycle for Advanced Reactor Applications. The authors would also like to thank Cliff B. Davis (INL) for his support of this work, specifically for incorporation of liquid salt properties into RELAP5-3D, and to Hussein S. Khalil and Edward A. Hoffman of ANL for their support in providing information on sodium cooled ABR design.

References

Adamov, E., Orlov, V., Filin, A., Leonov, V., Sila-Novitski, A., Smirnov, V., Tsikunov, V., 1997. The next generation of fast reactors. Nucl. Eng. Des. 173, 143–150.

Aquien, A., Kazimi, M.S., Hejzlar, P., 2006. Transuranics recycling in various reactor/fuel cycle systems. In: Transactions of the American Nuclear Society, vol. 95, Albuquerque, NM, USA, November 12–16.

Boardman, C.E., et al., 2000. A description of the S-PRISM plant. In: ICONE-8168, Proc. of ICONE-8, Baltimore, MD, USA, April 2–6.

Bonilla, C.F., 1958. Comparison of coolants. In: Etherington, H. (Ed.), Nuclear Engineering Handbook, pp. 9–90 (Sect. 9-3, Chap. 6.5).

Buiron, L., et al., 2007. Innovative core designs for Generation IV sodium-cooled fast reactors. In: Proc. International Congress on Advances in Nuclear Power Plants ICAPP'07, Nice, France, Paper 7383.

Dostal, V., Hejzlar, P., Todreas, N.E., 2004. Medium power lead alloy fast reactor balance of plant options. Nucl. Technol. 147 (September), 388–405.

Energy Solutions, 2008. GNEP deployment studies: overall summary report. Revision 1, No. DOE/NE/24503.1-1, May 19.

Gnielinski, V., 1976. New equations for heat and mass transfer in turbulent pipe and channel flow. Int. Chem. Eng. 16 (April (2)), 359–368.

GIF, 2002. A technology roadmap for Generation IV nuclear energy systems. GIF–002-00, December.

Handwerk, C.S., Driscoll, M.J., Hejzlar, P., 2006. Use of beryllium oxide to shape power and reduce void reactivity in gas-cooled fast reactors. In: PHYSOR 2006, Vancouver, Canada, September 10–14.

Handwerk C.S., Hejzlar P., Driscoll M.J., 2007. Core design and performance assessment for a supercritical CO_2-cooled fast reactor. MIT-ANP-TR-113, Center for Advanced Nuclear Energy Systems, Massachusetts Institute of Technology.

Hejzlar, P., Driscoll, M.J., Todreas, N.E., 2002. The long life gas turbine fast reactor matrix core concept. In: International Congress on Advanced Nuclear Power Plants, Hollywood, FL, June 9–13.

Hejzlar, P., Dostal, V., Driscoll, M.J., 2006. A supercritical CO_2 cycle—a promising power conversion system for Generation IV reactors. In: Proc. International Congress on Advances in Nuclear Power Plants ICAPP'06, Reno, NV, USA, Paper 6307, June 4–8.

Hoffman, E.A, Yang, W.S., Hill, R.N., 2006. Preliminary core design studies for the advanced burner reactor over a wide range of conversion ratios. ANL-AFCI-177, Advanced Fuel Cycle Initiative, Argonne National Laboratory.

Kambe, M., Uotani, M., 1998. Design and development of fast breeder reactor passive reactivity control systems: LEM and LIM. Nucl. Technol. 122 (May), 179.

Kubo, A., et al., 1997. Feasibility study on the reliable steam generator with helically coiled double wall tubes on FBR. In: ICONE5-2327, May 26–30.

Lee, J.I., Hejzlar, P., Saha, P., Stahle, P., Kazimi, M.S., McEligot, D.M., 2008. Deteriorated turbulent heat transfer of gas up-flow in a circular tube: experimental data. Int. J. Heat Mass Transf. 51, 3259–3266.

Mackay, F.J., Apostolakis, G., Hejzlar, P., 2008. Incorporating reliability analysis into the design of passive cooling systems with an application to a gas-cooled reactor. Nucl. Eng. Des. 238, 217–228.

Mizuno, T., Ogawa, T., Sugino, K., Naganuma, M., 2005. Advanced core design studies with oxide and metal fuels for next generation sodium-cooled fast reactors. In: Proc. International Congress on Advances in Nuclear Power Plants ICAPP'05, Seoul, Korea, Paper 5195, May 15–19.

Nikiforova, A., Hejzlar, P., Todreas, N.E., 2009. Lead cooled flexible conversion ratio fast reactor. Nucl. Eng. Des. 239, 2596–2611.

Ninokata, H., Sorokin, A.P., Kirillov, P.L., 2000. Comparison of sodium and lead/lead–bismuth as a coolant and LMFR safety. In: Proc. of 8th Int. Conf. on Nuclear Engineering, Baltimore, MD, USA, April 2–6.

OECD, 2000. Reduction of capital cost of nuclear power plants, OECD Nuclear Energy Agency Report.

Okada, K., 2008. Approach to FBR commercialization in Japan. In: Proc. International Congress on Advances in Nuclear Power Plants ICAPP'08, Anaheim, CA, USA, Paper 8397, June 8–12.

Patalano, G., Apostolakis, G.E., Hejzlar, P., 2008. Risk-informed design changes in passive decay heat removal system. Nucl. Technol. 163, 191–208.

Peterson, P.F., 2005. Roles and needs for simulation for the development of new reactors. In: Presentation at Nuclear Fuel Cycle Workshop, Lawrence Livermore National Laboratory, December 14–15.

Petroski, R., Hejzlar, P., Todreas, N.E., 2009. Liquid salt cooled flexible conversion ratio fast reactor. Nucl. Eng. Des. 239, 2612–2625.

Pope, M.A., Driscoll, M.J., Hejzlar, P., 2003. Reactor physics studies in support of GFR core design. In: Proc. of GLOBAL 2003, New Orleans, LA, USA, November.

Pope, M.A., Hejzlar, P., Driscoll, M.J., 2006. Thermal hydraulics of a 2400 MWt supercritical CO_2-direct cycle GFR. MIT-ANP-TR-107, Center for Advanced Nuclear Energy Systems, Massachusetts Institute of Technology.

Pope, M.A., Lee, J.I., Hejzlar, P., Driscoll, M.J., 2009. Thermal hydraulic challenges of gas-cooled fast reactors with passive safety features. Nucl. Eng. Des. 239, 840–854.

Spencer, B.W., 2000. The rush to heavy liquid metal reactor coolants—gimmick or reasoned. In: Proc. 8th Int. Conf. on Nuclear Eng., Baltimore, USA, April, pp. 2–6.

Shwageraus, E., Hejzlar, P., 2009. Liquid salt cooled flexible conversion ratio fast reactor: neutronic design, ibid.

Shwageraus, E., Hejzlar, P., 2008. Flexible conversion ratio lead cooled reactor design. In: Proc. Int. Conf. on the Physics of Reactors, PHYSOR'08, Interlaken, Switzerland, September 14–19.

Todreas, N.E., MacDonald, P.E., Hejzlar, P., Buongiorno, J., Loewen, E.P., 2004. Medium power lead alloy reactors—missions for this reactor technology. Nucl. Technol. 147 (September), 305–320.

Todreas, N.E., Kazimi, M.S., 1993. Nuclear Systems. I. Thermal Hydraulic Fundamentals. Hemisphere Publishing Corp.

Todreas, N.E., Hejzlar, P., Shwageraus, E., Petroski, R., Nikiforova, A., Fong, C.J., Whitman, J., 2008. Flexible conversion ratio fast reactor systems evaluations. Final Report, MIT-NFC-PR-101, Center for Advanced Nuclear Energy Systems, MIT, June.

Todreas, N.E., Hejzlar, P., Petroski, R., Nikiforova, A., Shwageraus, E., Fong, C.J., Dricoll, M.J., 2009. Flexible conversion ratio fast reactors: overview. Nucl. Eng. Des. 239, 2582–2595.

Wade, D.C., Chang, Y.I., 1988. The integral fast reactor concept: physics of operation and safety. Nucl. Sci. Eng. 100, 507–524.

Wade, D.C., Hill, R.N., 1997. The design rationale of the IFR. Prog. Nucl. Energy 31 (January (1)), 13–42.

Wade, D.C., Wigeland, R.A., Hill, D.J., 1997. The safety of the IFR. Prog. Nucl. Energy 31 (1–2), 63–82.

Williams, D.F., Toth, L.M., Clarno, K.T., 2006. Assessment of candidate molten salt coolants for the advanced high-temperature reactor (AHTR). ORNL/TM-2006/12, March.